[redacted]

NASA TECHNICAL MEMORANDUM

NASA TM X-984

NASA TM X-984

EXPERIMENTAL INVESTIGATION OF NOZZLE FLOW CHARACTERISTICS AND FORCES CONTRIBUTING TO TIPOFF OF THE SCOUT FOURTH-STAGE MOTOR(U)

by Earl H. Andrews, Jr., and Allen R. Vick

Langley Research Center
Langley Station, Hampton, Va.

NATIONAL AERONAUTICS AND SPACE ADMINISTRATION • WASHINGTON, D. C. • JULY 1964

[redacted]

EXPERIMENTAL INVESTIGATION OF NOZZLE FLOW CHARACTERISTICS AND FORCES CONTRIBUTING TO TIPOFF OF THE SCOUT FOURTH-STAGE MOTOR

By Earl H. Andrews, Jr., and Allen R. Vick

Langley Research Center
Langley Station, Hampton, Va.

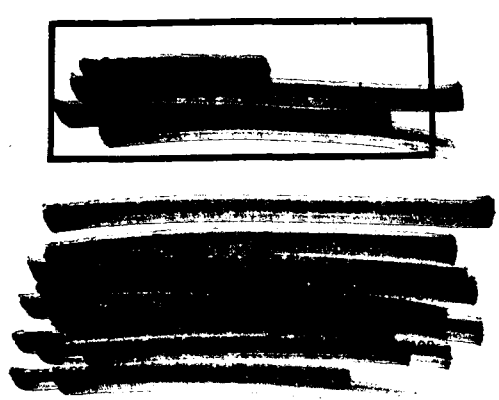

NATIONAL AERONAUTICS AND SPACE ADMINISTRATION

EXPERIMENTAL INVESTIGATION OF NOZZLE FLOW CHARACTERISTICS AND FORCES CONTRIBUTING TO TIPOFF OF THE SCOUT FOURTH-STAGE MOTOR*

By Earl H. Andrews, Jr., and Allen R. Vick
Langley Research Center

SUMMARY

15007

An investigation has been conducted to determine the flow characteristics of the fourth-stage nozzle of the Scout vehicle as a part of the overall study of the Scout "tipoff" problem. A full-scale model simulated the internal configuration of the Altair-IA5S rocket motor with a shortened nozzle. Nozzle static-pressure measurements were made during steady-state airflow studies and igniter firings in the simulator. Data obtained in a near-burnout simulation provide comparisons of the effects of propellant grain slots on the nozzle flow characteristics. Visual studies of the airflow in the nozzle inlet bell region were made by means of an oil-streak technique.

The oil-streak tests showed nonaxisymmetric flow in the vicinity of the nozzle inlet bell and also indicated that this lack of axisymmetry was a result of flow from the grain slots impinging on the inlet bell. The resulting flow disturbances within the nozzle produced nonuniform circumferential wall static-pressure distributions which resulted in small side forces. These forces alone would produce a flight-path tipoff angle well within the tolerance set for the Scout fourth stage. Conf. Rockar

INTRODUCTION

The practice of spin-stabilizing the final stages of solid-propellant multistage launch vehicles is well established. Although better stabilization could possibly be achieved by use of some types of reaction control system, the majority of the solid-propellant vehicles are so weight-critical that a guidance control system would impose a severe weight penalty. One of the problems associated with spin stabilization is the tendency of vehicles with such stabilization to veer off the planned flight path. With the advancement of multistage solid-propellant vehicles, such as the Scout, to the status of launch vehicles for orbital payloads, the tendency of the last stage to veer off the planned flight path results in erroneous orbital paths and may lead to complete failure to obtain payload orbit. Data analysis of previous flights of Scout

vehicles indicates that the tipoff of the last stage occurs during ignition and separation from the preceding stage (refs. 1 and 2). This tipoff problem may result from factors such as asymmetric failure of the separation plate employed, nonaxial expulsion of the nozzle closure plug at ignition, and/or asymmetric flows within the nozzle.

The investigation reported herein was initiated as a part of the overall study of the Scout tipoff problem with primary consideration being directed to a study of flows within the nozzle. The model used in this investigation simulated the internal configuration of an Altair-IA5S rocket motor at ignition. For comparison purposes, an additional configuration was investigated which simulated conditions near burnout, at which time the grain slots are eliminated. Because of the high ambient pressure of these tests, the nozzle was cut off at an area ratio of 4.00 in order to avoid nozzle flow separation due to nozzle overexpansion. Since the aerodynamic characteristics near the upstream end of the nozzle were of primary interest, the shortening of the nozzle was not considered to be detrimental to the investigation. The investigation was divided into two phases: The first phase consisted of static-pressure measurements during steady-state airflow tests with an air supply of approximately 450 psia at 100° F, and the second phase entailed the firing of igniters in an attempt to correlate airflow pressure measurements with those obtained during motor ignition. Both airflow and igniter tests were conducted with and without nozzle closure plugs. Also, visual studies of the airflow in the inlet bell region were conducted by means of an oil-streak technique.

SYMBOLS

A	area, in.^{2}
d	diameter, in.
F	force, lb
F_X	force acting along or parallel to X-axis, lb
F_Y	force acting along or parallel to Y-axis, lb
F_Z	force acting along or parallel to Z-axis, lb
I_X	roll moment of inertia, slug-ft^2
L	overall length of nozzle, in.
M	moment about center of gravity, in-lb or ft-lb
p_s	static pressure, psi
p_t	total pressure, psi

R radius, in.

s spin rate (angular velocity about the Z-axis), rad/sec or deg/sec

$T_{theor.}$ theoretical thrust, lb

t time, sec

z distance along nozzle center line from entrance lip, in.

$$\Delta P = \pi\left(\frac{p_s}{p_{t,c}} \cos \theta\right)_X \quad \text{or} \quad \pi\left(\frac{p_s}{p_{t,c}} \sin \theta\right)_Y$$

θ nozzle peripheral angle, deg

ψ slope of nozzle wall, deg

ϵ body tipoff angle (angular deflection of spin axis from reference axis), rad or deg

τ incremental time during which distributing force acts, sec

X,Y,Z longitudinal, lateral, and vertical axes

X',Y' X- and Y-axes through center of gravity

Subscripts:

c chamber

e exit

l local

r resultant

th throat

theor. theoretical

A bar over symbols indicates average value.

APPARATUS AND PROCEDURE

Models and Test Setup

A full-scale model of the Altair-IA5S rocket motor with a shortened nozzle (fig. 1(a)) was used in this investigation. An end view of the motor showing

the grain-slot arrangement in the propellant is shown in figure 1(b). Cold-air tests were conducted with this configuration using air at approximately 450 psia and at a total temperature of about 100° F. A quick opening valve (full open in about 0.3 second) permitted a rather rough simulation of the increase in chamber pressure with time, as would be produced by the firing of a flight igniter. In an effort to obtain comparisons with airflow tests, igniter firings were also conducted. A sketch of the simulator with an igniter installed in position is shown in figure 1(b) with the relative position of the igniter grain in relation to the main propellant slots shown in the insert. This igniter, as used in a previous investigation (ref. 2), was designed to produce a chamber pressure variation with time closely approximating that produced in actual flight. Another phase of this investigation included airflow tests of a near-burnout configuration of the motor with no grain slots (fig. 1(c)).

Both airflow and igniter tests were conducted with and without the standard lightweight styrofoam nozzle closure plugs. Figure 1(b) shows one of the plugs mounted in position. The hollow core of the plugs was filled with thermosetting adhesive in accordance with the procedure recommended for the flight motors. The plugs were set in place without cementing for the airflow tests but were cemented in place for the igniter tests as recommended by the manufacturer.

Instrumentation

Both total and static pressures were measured with pressure transducers having time lags in the order of a millisecond. The total pressure of the supply air was measured by a 500-psi pressure transducer located just upstream of the grain slots in the chamber (fig. 1(a)). For the igniter tests, the transducer was vented to the chamber through the mounting shaft of the igniter paddle (fig. 1(b)); in the near-burnout simulator, total pressure was measured upstream of the nozzle (fig. 1(c)).

The nozzle was instrumented with a total of 26 static-pressure orifices as shown in figure 2(a). Twelve static-pressure orifices were located in line from the inlet bell to the nozzle exit; and two rings of eight orifices, one each at the throat and exit stations, were used to obtain circumferential pressure distributions. Total- and static-pressure survey rakes (fig. 2(b)) were used to survey immediately downstream of the nozzle throat. The location of the seven-probe total-pressure rake was chosen to prevent blockage effects. Static-pressure measurements were made with a three-probe rake located in the same relative position as the total-pressure survey rake. All pressure measurements were continuously recorded on an oscillograph.

Visual Flow Studies Techniques

Visual studies within the nozzle were conducted by using an oil-streak method. Dots of a lampblack-oil mixture were applied in rings to the nozzle, as shown in the typical pretest photographs of figure 3(a). The results were recorded for further analysis by use of photographs and a permanent mold. The permanent mold incorporated a new technique which is described in the appendix.

RESULTS AND DISCUSSION

All pressures, forces, and moments are presented in a nondimensional form and were obtained from a steady-state airflow test. The test was of sufficient duration to enable the total pressure to reach the programed value and produce a more-or-less steady-state flow for a period of approximately 3 seconds from which data are presented for a 1-second period. The discussion which follows includes the results and analysis of a visual oil-flow study, the static-pressure distribution in the nozzle, the steady-state airflow test, and the tipoff angle.

Visual Flow Studies

Oil-streak studies.- Visual studies were conducted during the airflow tests by using an oil-streak technique; the results of these studies are shown in figure 3. Typical posttest photographs of the oil-streak specimens for the grain-slot simulation are shown in figures 3(b), 3(c), and 3(d). Side and end views shown in figures 3(b) and 3(c), respectively, are incorporated in a composite photograph (fig. 3(d)). The oil patterns of these photographs show considerable nonaxisymmetric airflow on the external surface of the nozzle inlet bell (fig. 3(b) and areas A and B in fig. 3(d)). The flow direction was downstream into the blind corner (see B in fig. 1(a)) in the region downstream of the shallow grain slots (views II and IV of fig. 3(b)) and upstream in the areas between adjacent deep slots (views I and III of fig. 3(b)). Permanent mold records made of the oil-streak patterns showed circumferential flow on the lip of the nozzle inlet bell in the region between adjacent deep slots. This circumferential flow ended abruptly at the outer edge of the deep slots and flowed into the nozzle inlet bell, as indicated in figure 3(c) by the lines of oil extending from the nozzle lip to the throat. The presence of only three lines, indicated by a, b, and d in figures 3(c) and 3(d), instead of four (there should be one at c) indicates a possibility of flow detachment since the oil dots were applied as consistently and uniformly as possible.

The posttest photograph for the near-burnout simulation (fig. 3(e)) shows that the oil dots on the external surface of the inlet bell are undisturbed and that the flow about the lip of the inlet and inside the nozzle is axisymmetric. Therefore, it may be concluded that the previously discussed deviation from axisymmetric airflow on the external surface of the inlet bell is the direct result of the flow emitting from the slots and impinging upon this surface.

Nozzle erosion.- The presence of nonaxisymmetric flow in the region of the nozzle inlet bell was further indicated during one of the igniter tests in which "chuffing" occurred. Following the main igniter firing, which lasted for approximately 0.12 second and produced a chamber pressure of 360 psia, a single "chuff" occurred about 1.67 seconds later, lasted for about 0.07 second, and produced a maximum chamber pressure of 185 psia. This "chuffing" resulted in the erosion of areas of the steel nozzle, as shown in figure 4. The propellant grain slots are superimposed on the photograph to show the relative position of the eroded areas with respect to the grain slots. The four heavily eroded areas

indicate that the flow approaching the inlet bell has symmetry with respect to the grain pattern but that it is not axisymmetrical. The areas of erosion suggest areas of high heating and turbulence.

Deposits on the nozzle following an igniter firing are shown in figure 5. The residue consists mainly of the aluminum oxide contained in the propellant. The ridge visible on the external surface of the nozzle inlet bell of figure 5(a) is the unburned residue of the cement utilized in the installation of a nozzle closure plug. The cement showed little sign of melting during the igniter test, although during an actual motor firing it would probably be melted and dispersed. Residue produced by the igniter alone is shown in figure 5(b). Effects of the deep grain slots are readily evident in that heavy concentrations of slag are left on the external surface of the nozzle adjacent to these slots.

Pressure Distributions

In-line pressures.- Typical pressure distributions, obtained during an airflow test, along a line originating on the lip of the inlet bell and extending down the nozzle to the exit are shown in figure 6. The two sets of data for each chamber pressure, which were obtained from different tests having conditions as nearly equal as possible, show slight differences between the two positions of the static-pressure orifices relative to the grain slots. For comparison purposes, the theoretical pressure distributions determined from the nozzle area ratios are also shown. At the lower chamber pressure, flow separation exists within the nozzle due to overexpansion; however, this condition is eliminated at the higher pressures. In all these tests the effective throat of the nozzle is approximately 0.25 inch upstream of the geometric throat.

Circumferential pressures.- Several typical static-pressure distributions obtained around the nozzle geometric throat at different total pressures, and consequently varying time intervals, are shown in figure 7. The distributions for the grain-slot simulation with a smooth nozzle are presented in figure 7(a) with the slot arrangement shown superimposed on the distributions for the lowest pressure. The data for the two lowest pressures were obtained before the chamber pressure had reached a near constant peak value; the remaining four distributions were obtained during the near-constant chamber pressure portion of the test. Although asymmetric distributions are evident at all chamber pressures, of particular interest are the curves for $p_{t,c} = 430$ and 437 psia for which the same total pressure occurred at different times. These particular throat distributions show an apparent pulsation of the pressures and also a shift in location of the peak distribution. The curves for $p_{t,c} = 430$ psia show an approximate 10-percent variation in pressure ratio which corresponds to a change in Mach number from about 1.19 to 1.27. The effects of these variations in pressure and the contribution to side forces are shown in the steady-state test analysis.

Efforts to obtain pressure distributions during an igniter firing were unsuccessful, due to the formation of deposits in the nozzle which resulted in partial blockage of the pressure orifices and varying time lag. However, airflow tests were conducted with the nozzle coated with slag from an igniter

firing (fig. 5(b)). The results of these tests are shown in figure 7(b), where the presence of asymmetric pressure distributions within the nozzle are again evident. As was evident in the smooth nozzle results, there is an apparent pulsation of the pressures and also a shift in location of the peak pressures from one time to another for the same total pressure.

Pressure distributions for the airflow through a smooth nozzle of the near-burnout simulator (fig. 1(c)) are presented in figure 7(c). Although considerable improvement is noted in the distributions as compared with those in figures 7(a) and 7(b), there is still evidence of asymmetric flow.

Rake surveys.- Total-pressure surveys just downstream of the nozzle throat were conducted to determine the effect of the grain slots and abrupt inlet bell upon the pressures measured in the nozzle. The results of these total-pressure distributions are presented in figure 8 with the rake positions superimposed on the grain-slot arrangement at the top of each set of curves. Local total pressures across the measuring station are divided by the chamber total pressures for a series of chamber pressures. It is obvious that the distributions of $p_{t,l}/p_{t,c}$ are far from ideal. The existence of pressure ratios greater than 1.0 indicates that the chamber total pressure measured at a single station does not represent an average stagnation pressure. Additional distributions shown in figures 8(b) and 8(c) with different rake orientations relative to the grain slots fail to show any distinct effects of slot orientation.

Typical surveys of static pressure and total pressure are shown in figure 9(a) for three rake positions. Local Mach numbers corresponding to the measured pressure ratios, tabulated in figure 9(a), show a considerable variation across the nozzle, ranging from 1.07 at the nozzle center line to 1.41 near the wall. A pictorial contour sketch of the total-pressure profiles used in figure 9(a) is shown in figure 9(b).

Steady-State Airflow Tests

The discussion thus far has been limited to establishing the nature of the flow within the nozzle. In order to determine whether the asymmetry which was found to exist was of sufficient magnitude to produce forces capable of causing tipoff, a representative steady-state airflow test was chosen for thorough analysis, the results of which are presented in the following paragraphs and in figures 10 to 15.

Radial forces.- Complete circumferential pressure distributions were measured at the throat and exit stations. Corresponding vertical and lateral forces per unit area were then determined. (See fig. 10 for typical distributions.) The variation of the unit area forces $\pi\left(\frac{p_s}{p_{t,c}} \cos\theta\right)_X$ or $\pi\left(\frac{p_s}{p_{t,c}} \sin\theta\right)_Y$ nondimensionalized with respect to the local pressure coefficient, was assumed to be a linear function of the local pressure coefficient (fig. 11). Data from

plots such as figure 11 were then used to determine the vertical- and lateral-force distributions which, when integrated along the nozzle (fig. 12), resulted in side-force components.

The data were processed for a 1-second time interval to determine whether the pressure variation would average to zero after many cycles. Figure 13 shows that no such tendency exists. An integration of these forces (fig. 13) over the 1-second period resulted in small but significant side-force components $\frac{\overline{F_X}}{T_{theor.}} = 0.00597$ and $\frac{\overline{F_Y}}{T_{theor.}} = -0.00288$ which yielded a resultant side force of $\frac{F_r}{T_{theor.}} = 0.00667$. The components and resultant force are presented in figure 14 with the grain slots shown superimposed.

Moments.- The existence of asymmetric side forces on a rocket motor in flight results in moments about the center of gravity of the motor. Results from this investigation are therefore converted to moments about the center of gravity. Since it is believed that most of the asymmetric pressure disturbances occur during the ignition of the rocket motor, the moment arm utilized was that of a fully loaded motor and its payload and was obtained from reference 3 for the Scout vehicle designated ST-1.

The moment components obtained at several intervals during the 1-second analysis period were integrated with respect to time to obtain a time-averaged value for the components $M_{X'}$ and $M_{Y'}$. Again no tendency existed for the moments to average to zero. Figure 15 presents a sketch showing these moments and all the contributing forces. (The moment components were treated as vectors in order to obtain a resultant moment which was on the order of 1.59 in-lb/psi of chamber total pressure.)

Tipoff angle.- The preceding analysis did not account for any stabilization effects due to the spin rate of the vehicle. However, by referring to the analysis of reference 4, which takes into account the spinning motion, and utilizing the herein reported resultant moment, a body tipoff angle may be obtained. The data of references 4 and 5 were the basis for the selection of the spin rate s, the moment of inertia I_X, and a reasonable time period τ. The body tipoff angle expressed in degrees is computed as follows:

$$\epsilon = \frac{2M}{I_X s^2} \sin \frac{s}{2} \tau$$

$$\epsilon = \frac{2(33.1)}{6.25(18.64)^2} \sin \frac{1068(0.05)}{2}$$

$$\epsilon \approx 0.014 \text{ radian} \approx 0.79^{\circ}$$

where

$$M = \frac{\overline{M_r}}{p_{t,c}} p_{t,c} \approx 33.1 \text{ ft-lb}$$

$$p_{t,c} = 250 \text{ psi}$$

$$I_X = 6.25 \text{ slug-ft}^2$$

$$\tau = 0.05 \text{ sec}$$

$$s = 178 \text{ rpm} = 1068 \text{ deg/sec} = 18.64 \text{ radians/sec}$$

The foregoing computations resulted in an approximate body tipoff angle of 1.0°. Choice of time to obtain the largest possible sine function in the tipoff-angle equation results in a greater body tipoff angle of 2.0°. For the Scout launch vehicle, a generally accepted criterion is that the body tipoff angle of the fourth stage (Altair-IA5S) is four times the flight-path tipoff angle which has a tolerance of 0.6°. Therefore, the results of this investigation indicate that although asymmetrical nozzle flows exist, the resultant forces are small and contribute very little to the Scout fourth-stage flight-path tipoff angle.

CONCLUSIONS

An investigation has been conducted of a simulated rocket motor to determine the flow characteristics of the fourth-stage nozzle of the Scout vehicle. From the results of this investigation, the following conclusions were drawn:

1. In the presence of the fuel grain slots, oil-streak studies showed nonaxisymmetric flow existing in the vicinity of the nozzle inlet bell. The oil pattern features indicated that the impingement of the flow from the grain slots on the inlet bell was responsible for this deviation from axisymmetrical flow.

2. Erosion in the nozzle inlet bell during an igniter firing in which "chuffing" occurred suggested areas of high heating and turbulent flow.

3. Flow disturbances within the nozzle produce nonuniform circumferential wall static-pressure distributions capable of producing small side forces which

result in a flight-path tipoff angle well within the tolerance set for the Scout fourth stage.

Langley Research Center,
National Aeronautics and Space Administration,
Langley Station, Hampton, Va., March 3, 1964.

APPENDIX

A METHOD OF OBTAINING HIGH CONTRAST PERMANENT RECORDS OF SURFACE FLOW PHENOMENA

The general purpose for the development of this method was the necessity for making undistorted and detailed permanent records of surface flow phenomena. Visual determination of surface flow phenomena by the oil-streak technique, utilizing a mixture of lampblack and oil, is well known and has been used over a considerable period of time. Although photographs may be made to record this visual information, a considerable amount of detail is lost and distortions are evident in making composite photographs. Inaccessible locations and complex internal shapes also prohibit or limit the use of photographs. The existing problem of concern was, therefore, how to lift the oil smears from the surface of a model in such a manner as to obtain a permanent record, rather than how to apply the oil and lampblack solution or how to obtain the oil smears.

During this investigation, a solution to the problem was found which completely satisfied all requirements. A liquid compound was found which could be easily applied, allowed to set up and harden, and then removed from the model with the oil-streak pattern intact on the mold. The liquid is a commercially available product, a room-temperature-vulcanized silicone rubber with a catalyst added. Not only are the oil streaks lifted from the surface of the model without smudging but the rubber mold completely absorbs the oil and retains each minute detail. Absorption is complete to such an extent that the model surface is clear of all traces of the oil smears after removal of the rubber mold. After drying for a few hours, the mold with its pattern of oil is almost smudge proof. Since the rubber is white, sharp contrast is obtained with the oil and lampblack solution.

REFERENCES

1. Young, George R., and Buglia, James J.: An Analysis of the Coning Motions of the Final Stages of Three NASA Scout Development Vehicles. NASA TN D-1396, 1962.

2. Gungle, Robert L., Brosier, William S., and Leonard, H. Wayne: An Experimental Technique for the Investigation of Tipoff Forces Associated With Stage Separation of Multistage Rocket Vehicles. NASA TN D-1030, 1962.

3. Mayhue, Robert J., Compiler: NASA Scout ST-1 Flight-Test Results and Analyses, Launch Operations, and Test Vehicle Description. NASA TN D-1240, 1962.

4. Suddath, Jerrold H.: A Theoretical Study of the Angular Motions of Spinning Bodies in Space. NASA TR R-83, 1961.

5. Buglia, James J., Young, George R., Timmons, Jesse D., and Brinkworth, Helen S.: Analytical Method of Approximating the Motion of a Spinning Vehicle With Variable Mass and Inertia Properties Acted Upon by Several Disturbing Parameters. NASA TR R-110, 1961.

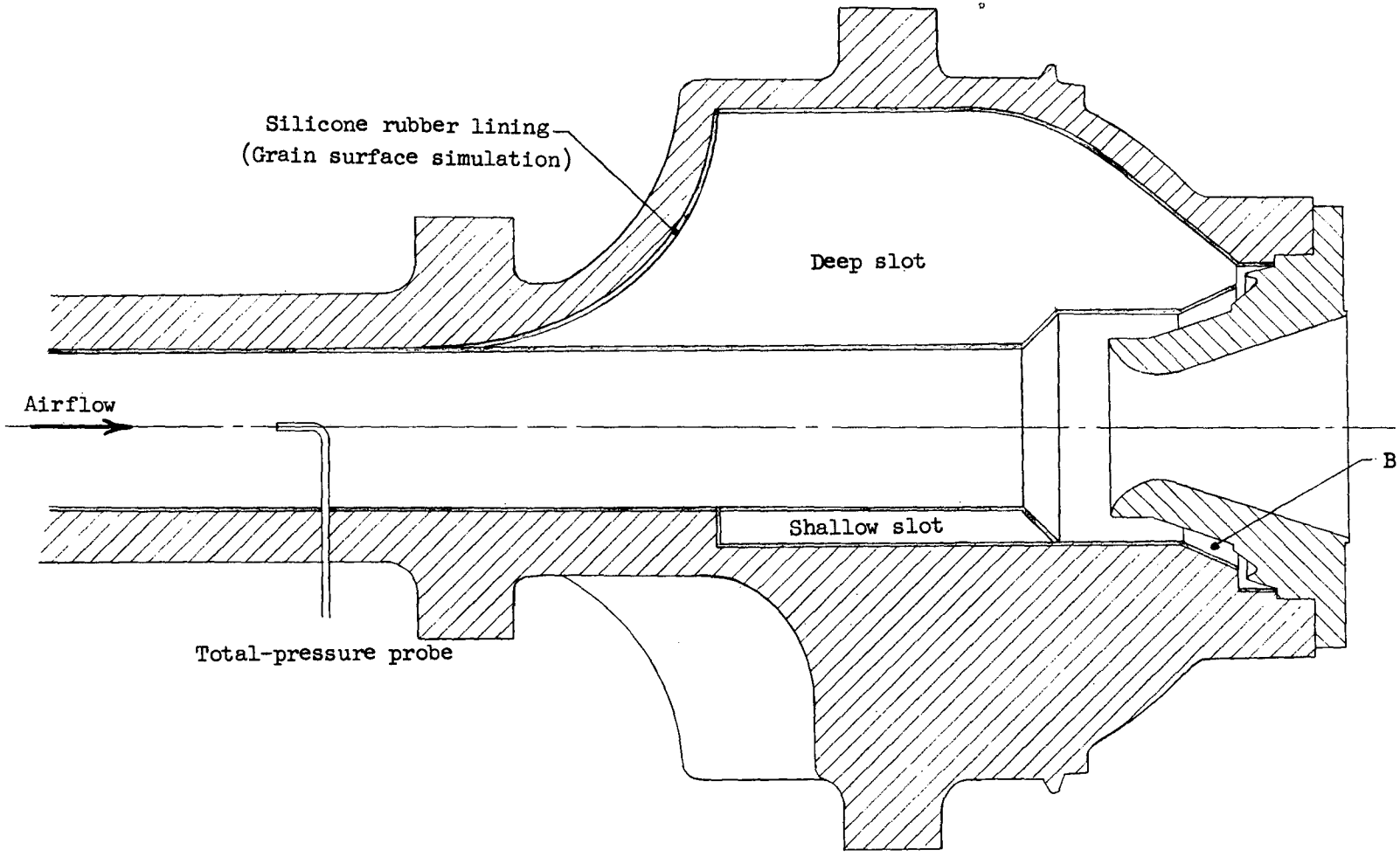

(a) Overall view of simulator using air.

Figure 1.- Altair-IA5S rocket motor simulator; $\frac{A_e}{A_{th}} = 4.00$.

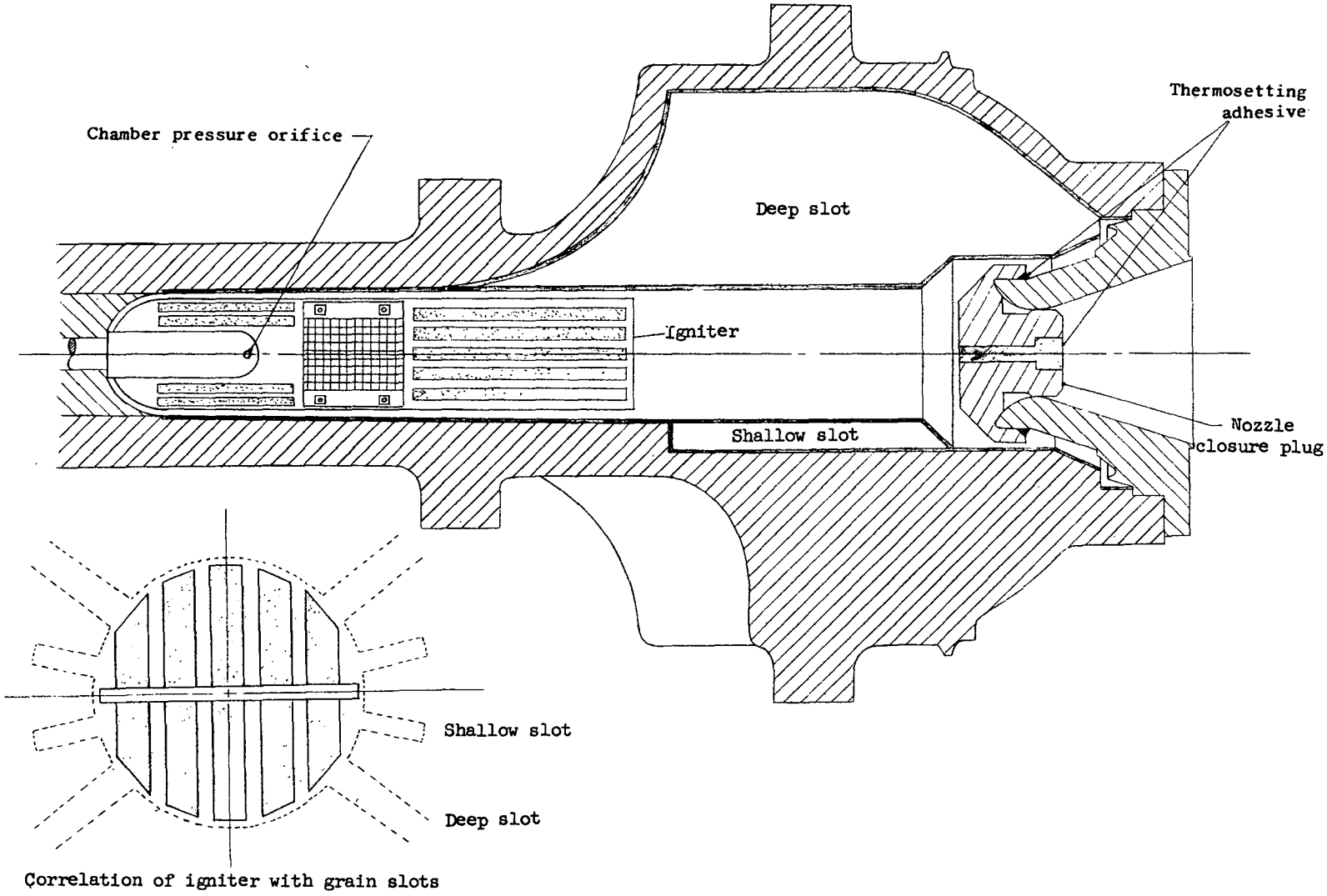

(b) Overall view of simulator employing an igniter.

Figure 1.- Continued.

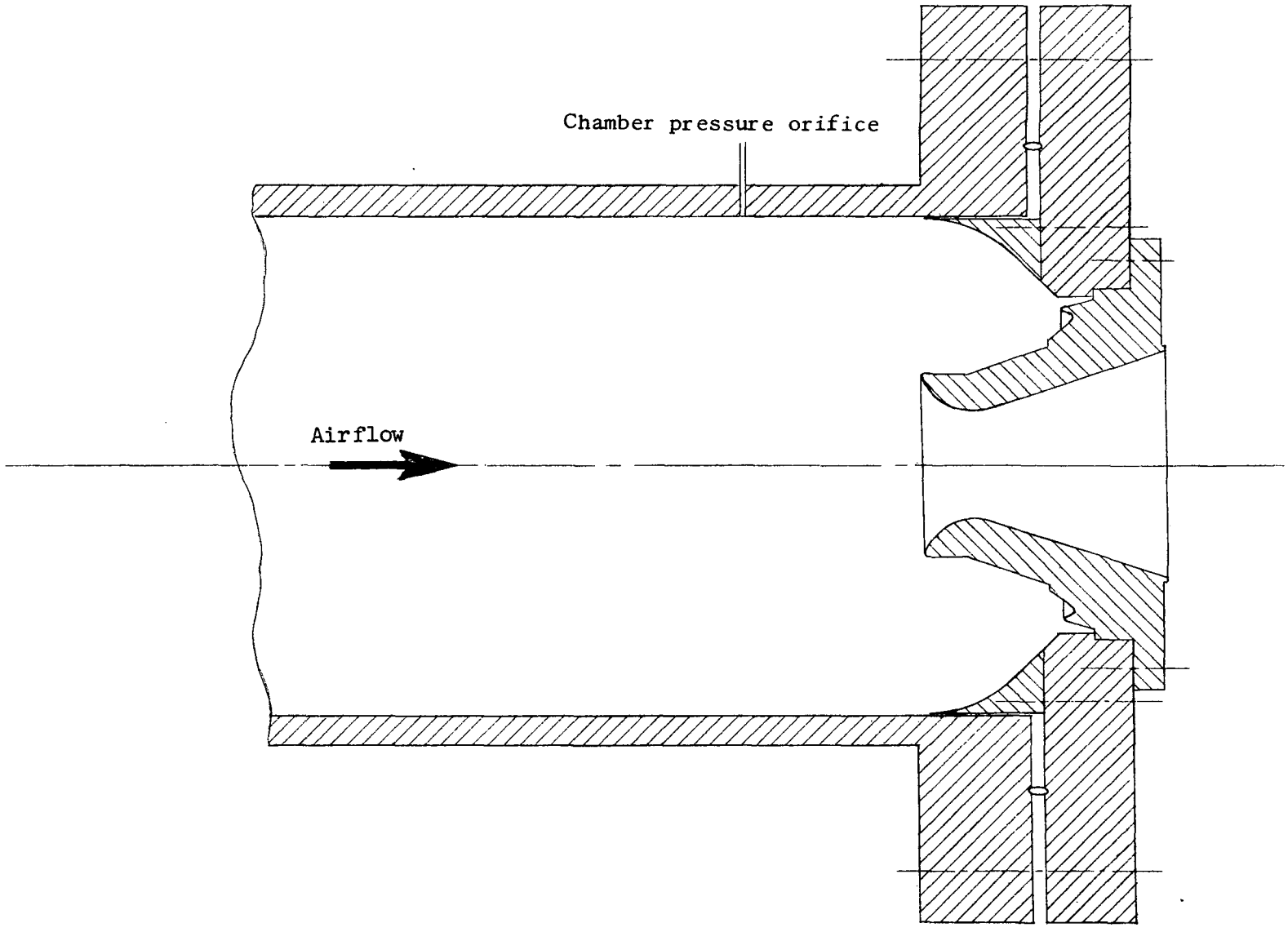

(c) Near-burnout simulator.

Figure 1.- Concluded.

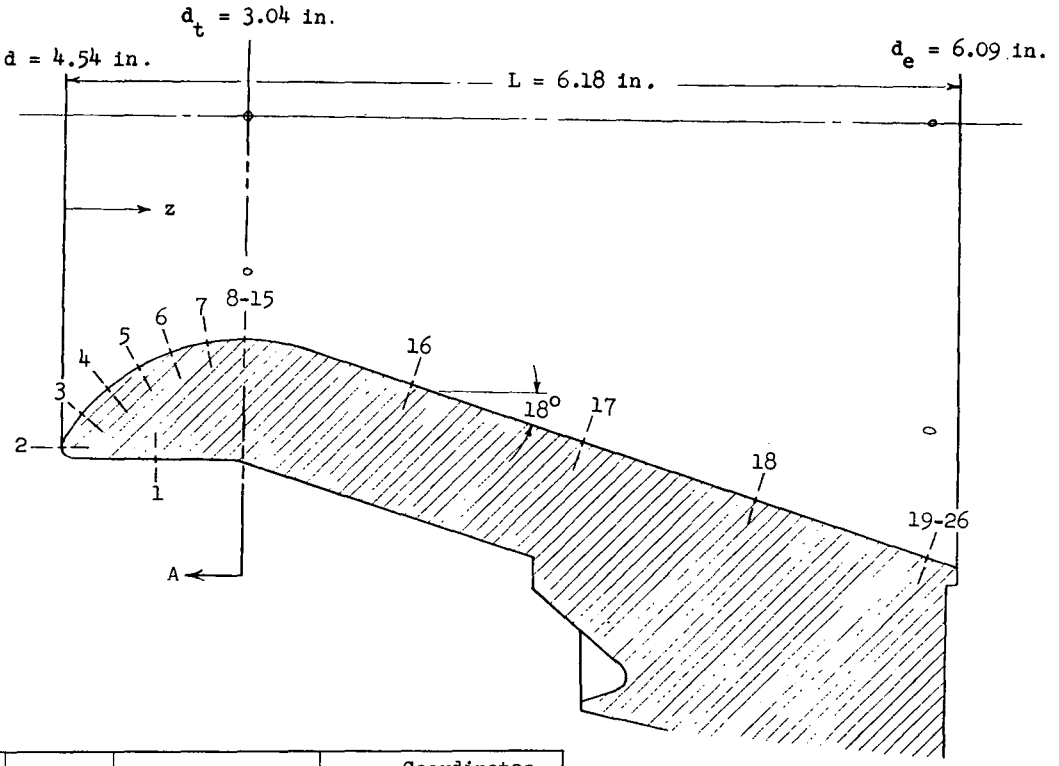

Orifice No.	θ, deg	Local wall slope, ψ, deg	Coordinates R/R_{th}	Coordinates z/L
1	0	0	1.55	.10
2		90	1.49	0
3		50	1.34	.02
4		40	1.22	.05
5		30	1.13	.09
6		20	1.06	.12
7		10	1.01	.16
8		0	1.0	.205
9	45			
10	90			
11	135			
12	180			
13	225			
14	270			
15	315			
16	0	18	1.19	.38
17			1.43	.57
18			1.70	.77
19			1.96	.97
20	45			
21	90			
22	135			
23	180			
24	225			
25	270			
26	315			

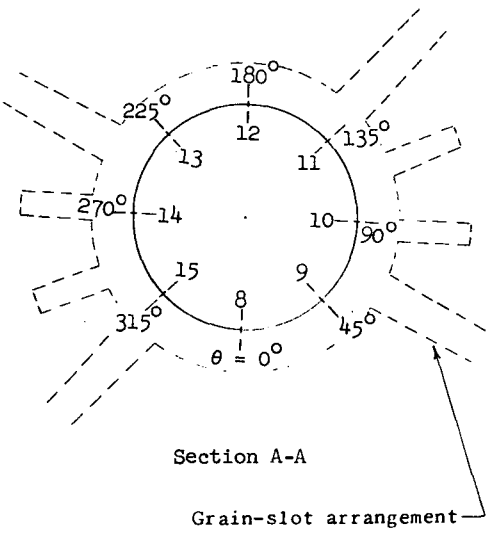

(a) Nozzle geometry and instrumentation.

Figure 2.- Pressure instrumentation.

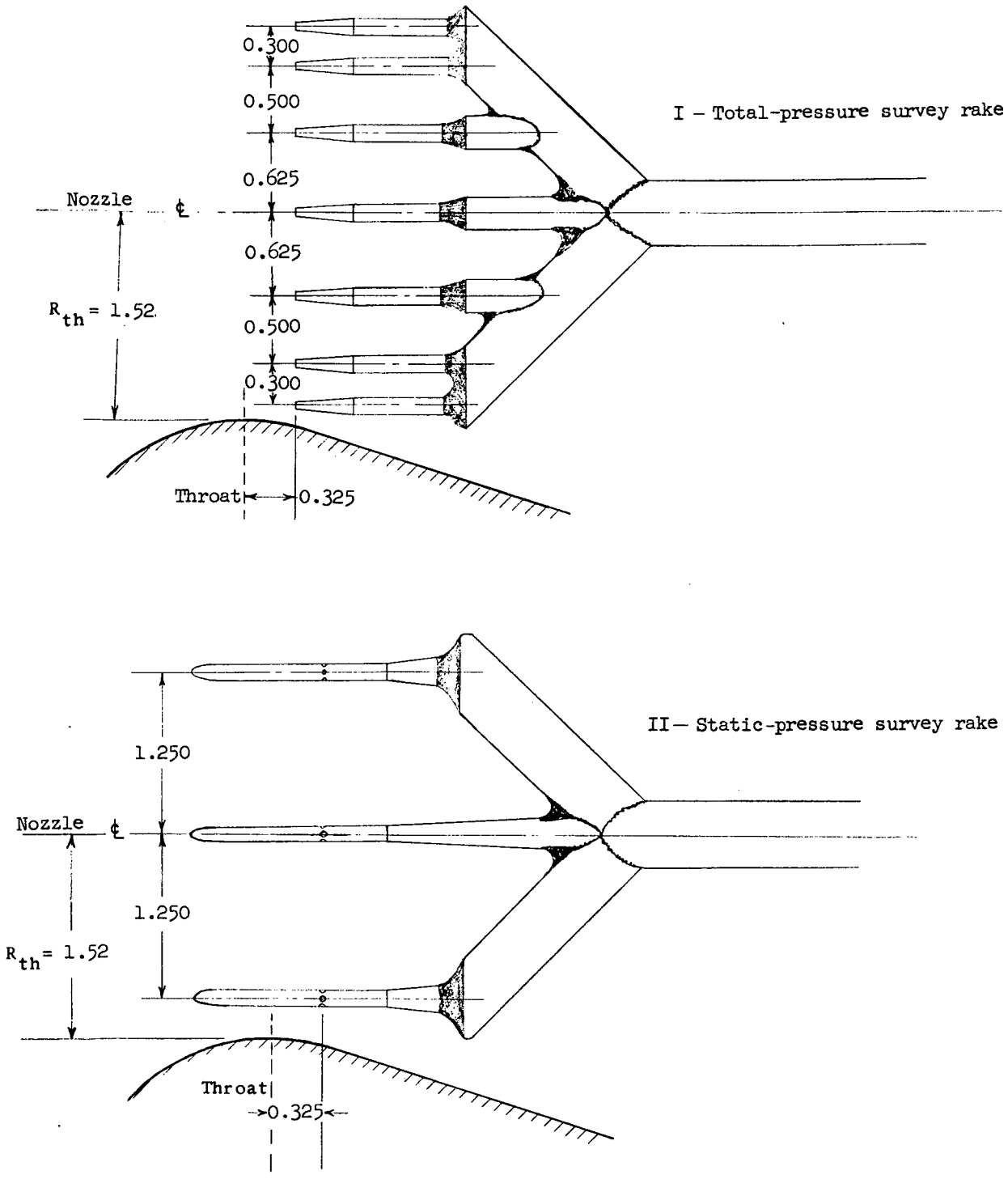

(b) Nozzle survey rakes. All dimensions are in inches.

Figure 2.- Concluded.

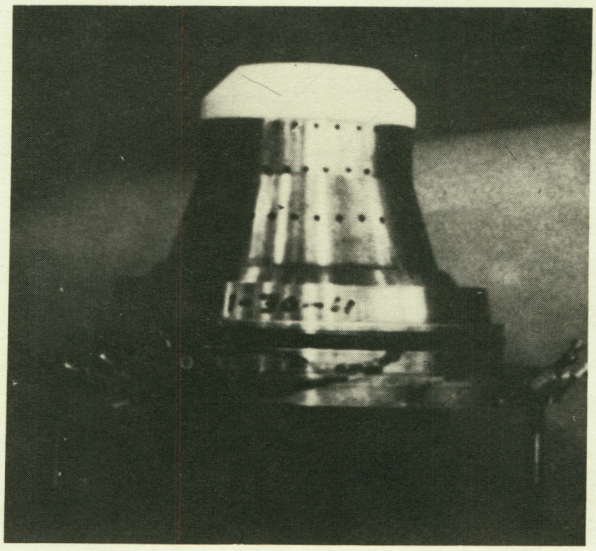

Side view L-62-5778

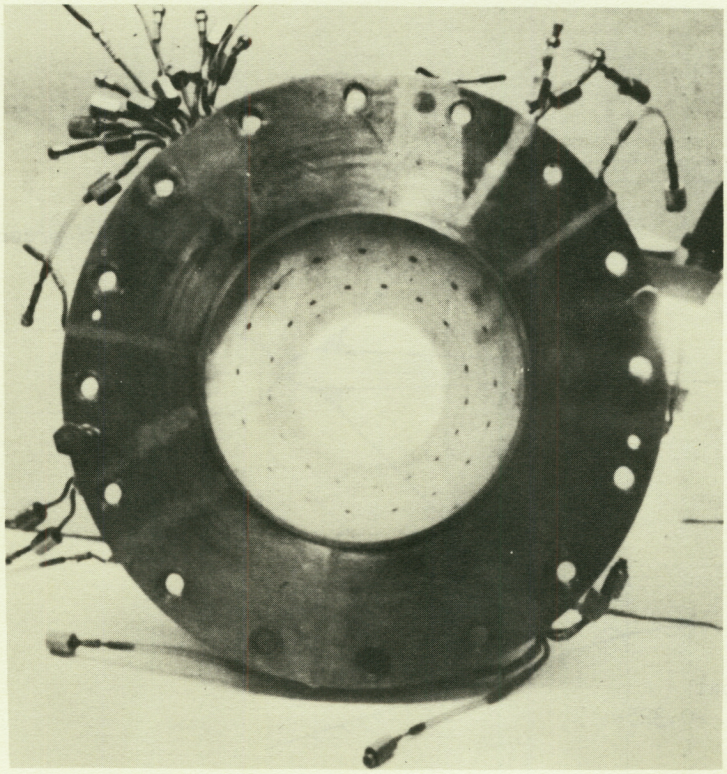

Exit view L-62-5777

(a) Typical pretest views.

Figure 3.- Pretest and posttest views of nozzles for oil-streak studies.

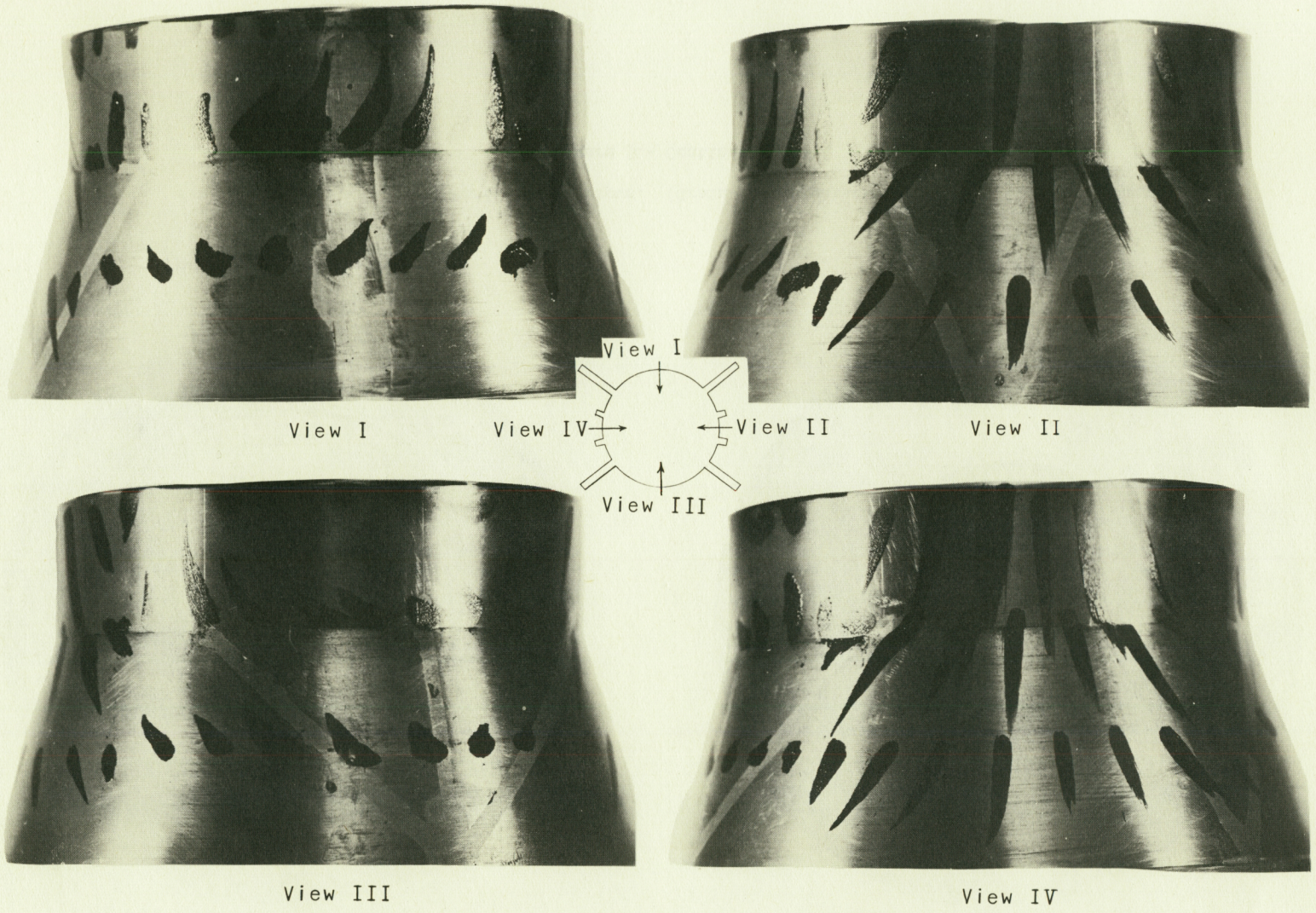

(b) Posttest side views. (Grain-slot simulation.) L-64-3009

Figure 3.- Continued.

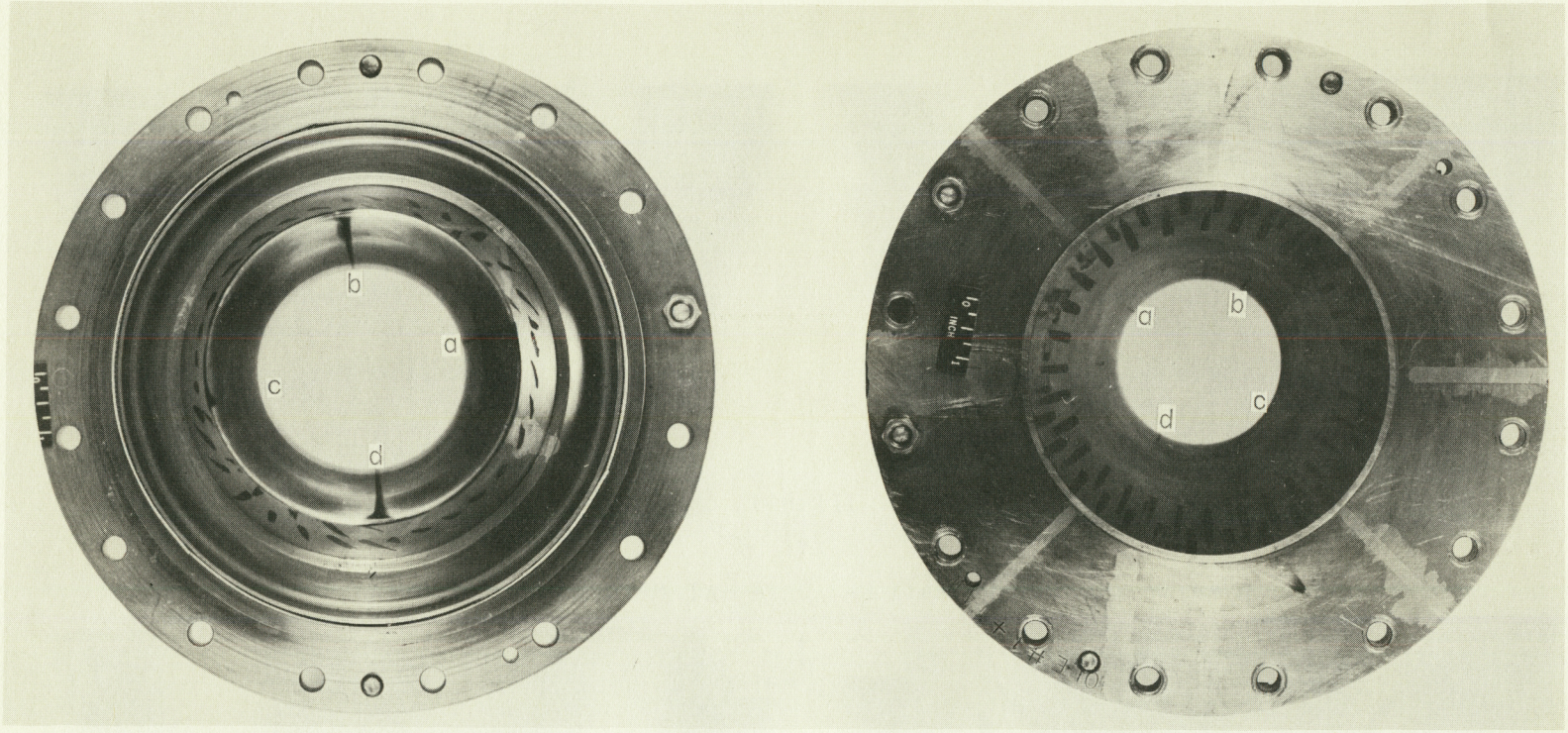

Inlet bell view

Exit view

(c) Posttest end views. (Grain-slot simulation.) L-64-3010

Figure 3.- Continued.

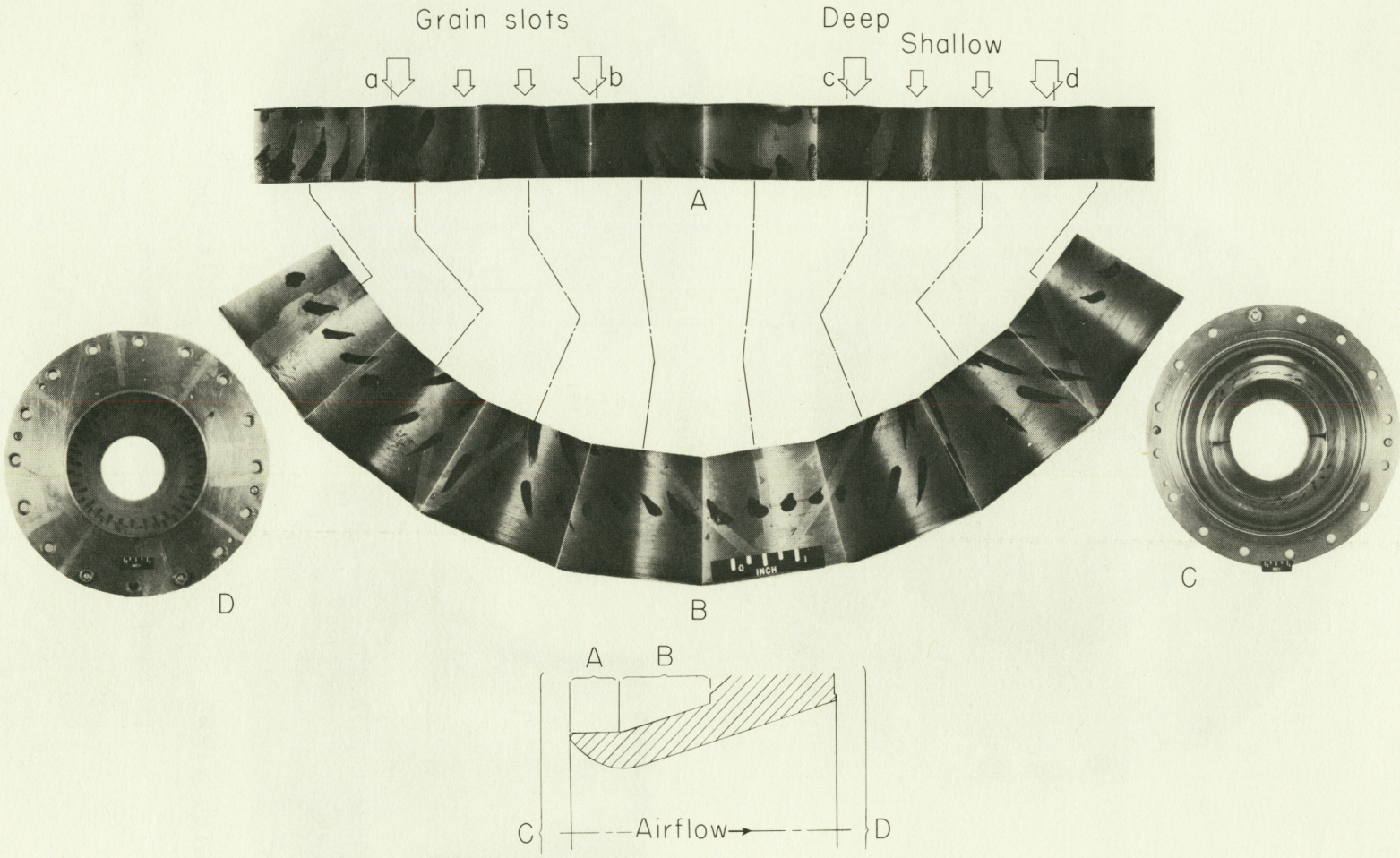

(d) Posttest composite. (Grain-slot simulation.) L-64-3011

Figure 3.- Continued.

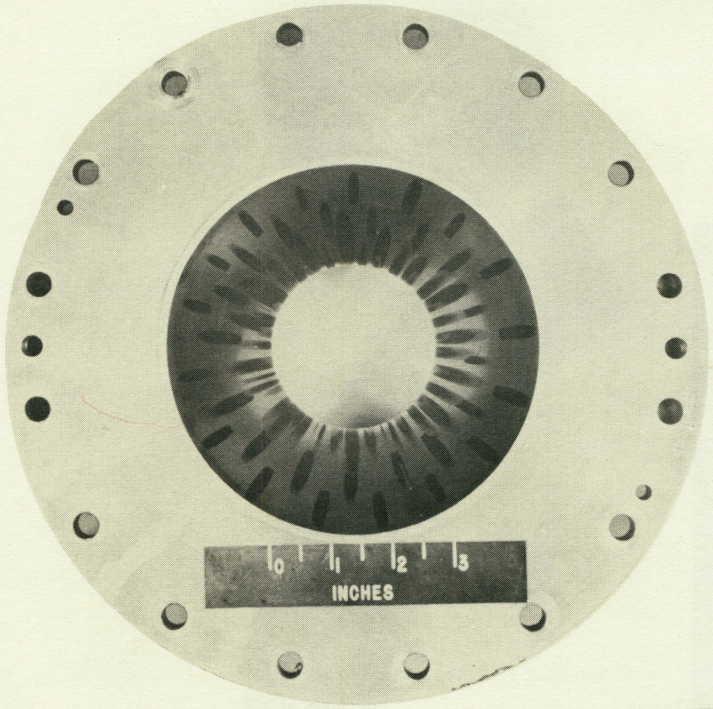

Exit view

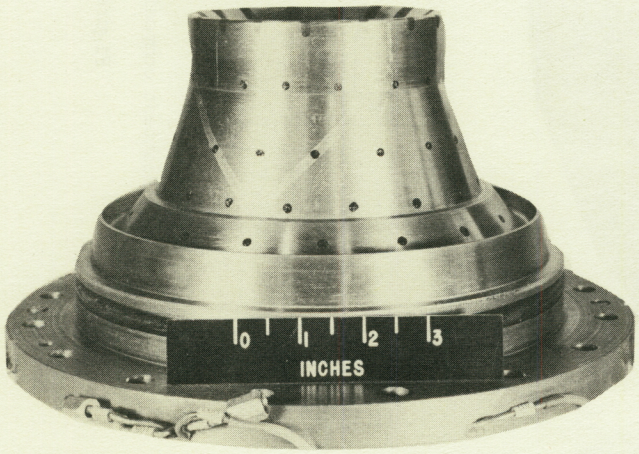

Side view

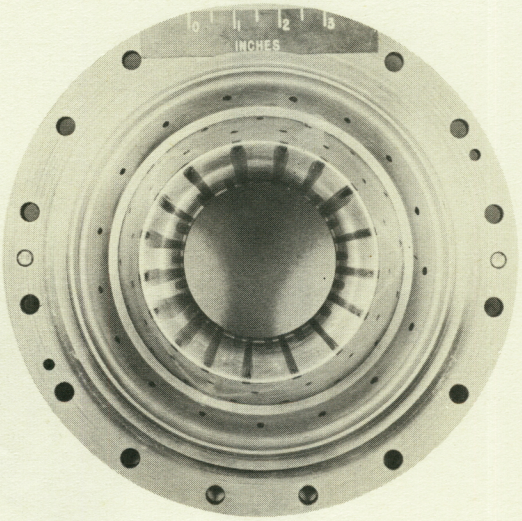

Inlet bell view

(e) Posttest views of near-burnout simulation. L-64-3012

Figure 3.- Concluded.

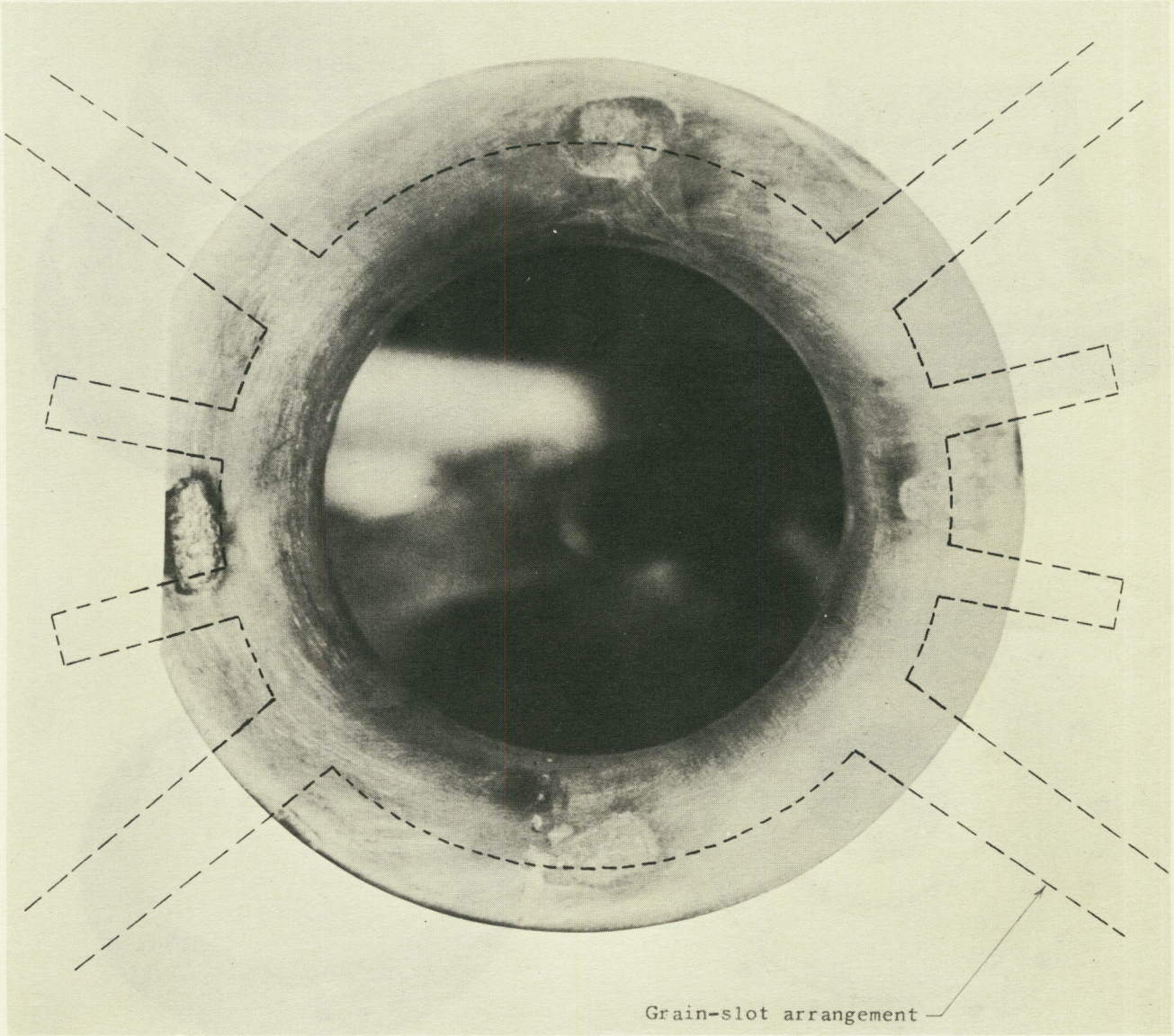

L-64-3013

Figure 4.- Nozzle inlet bell showing erosion due to hot gases emitting from igniter.

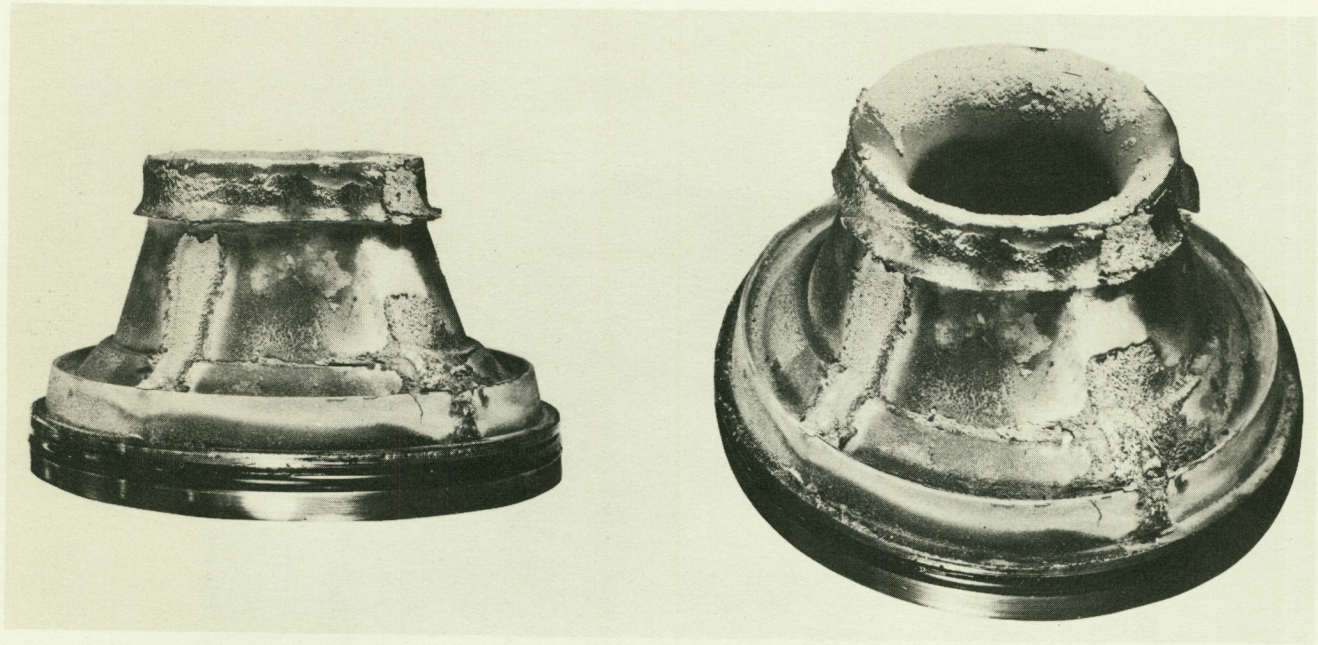

(a) Nozzle showing ridge of unburned cement.

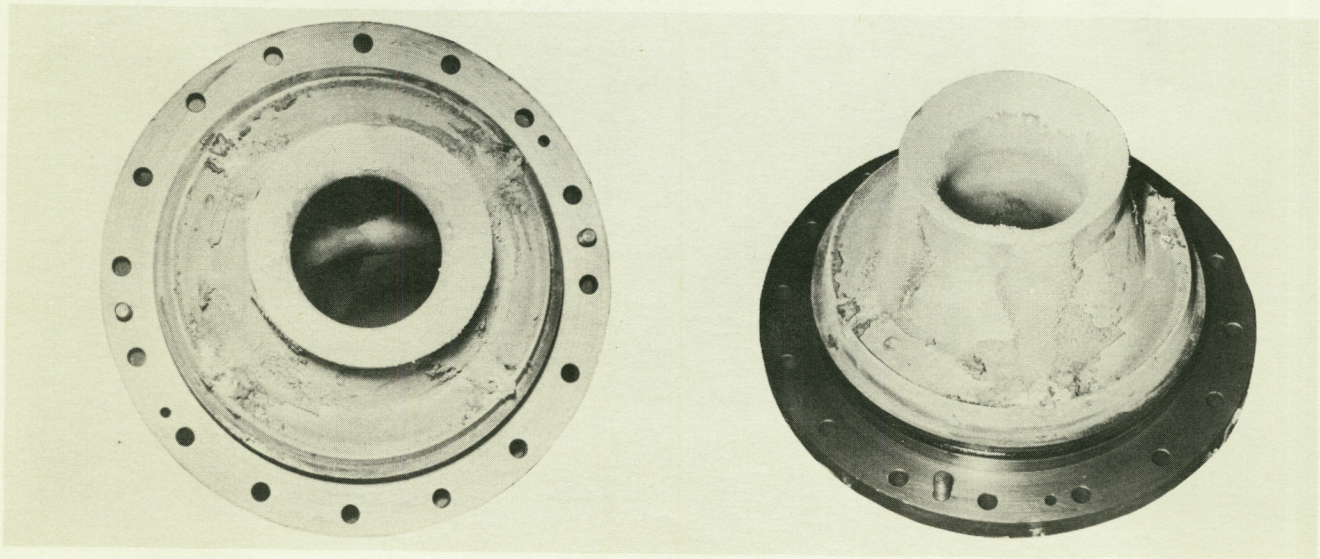

(b) Residue-deposited nozzle used in an airflow test. L-64-3014

Figure 5.- Residue deposited on nozzle as a result of igniter firing.

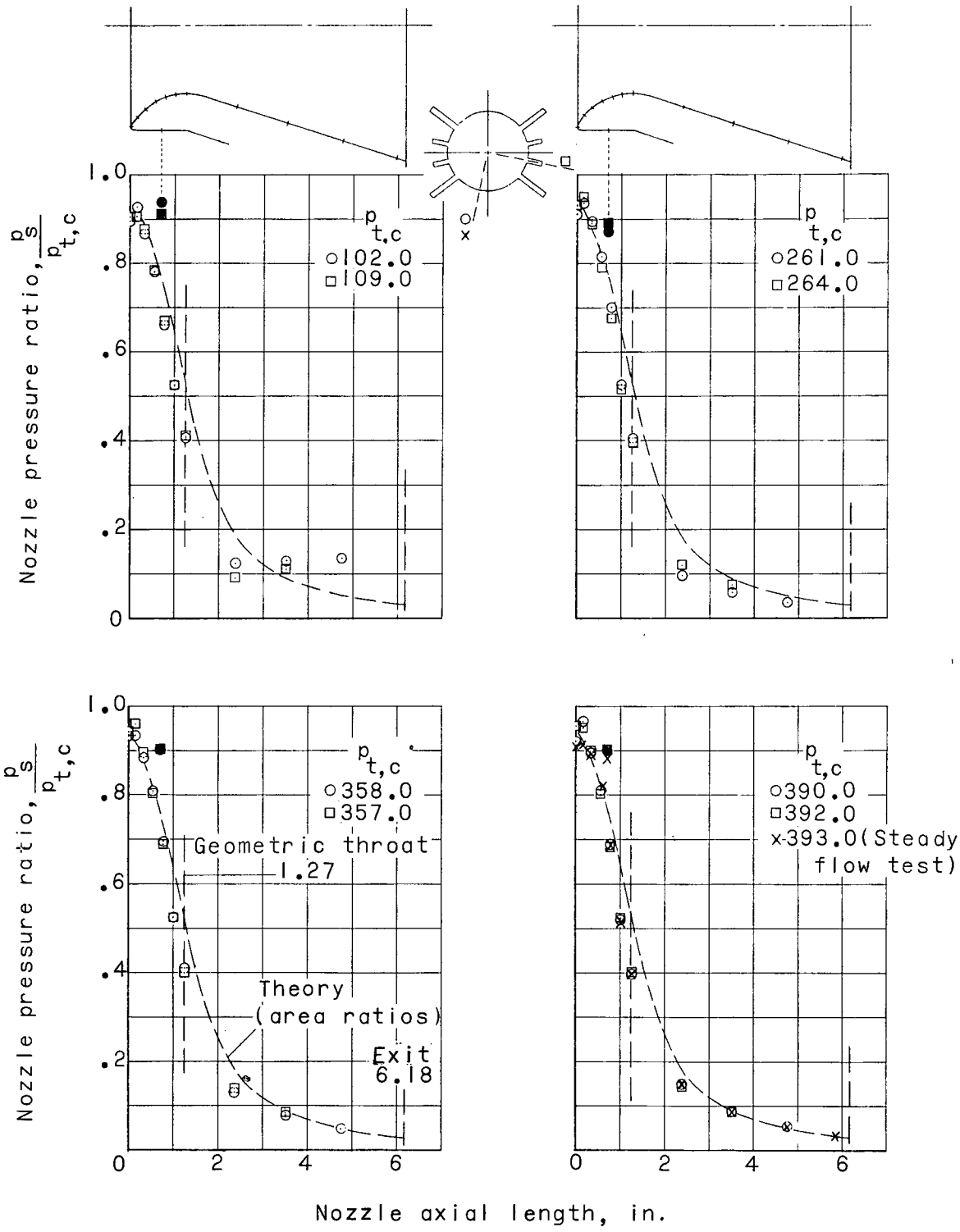

Figure 6.- Static-pressure distributions from inline orifices over the length of the nozzle.

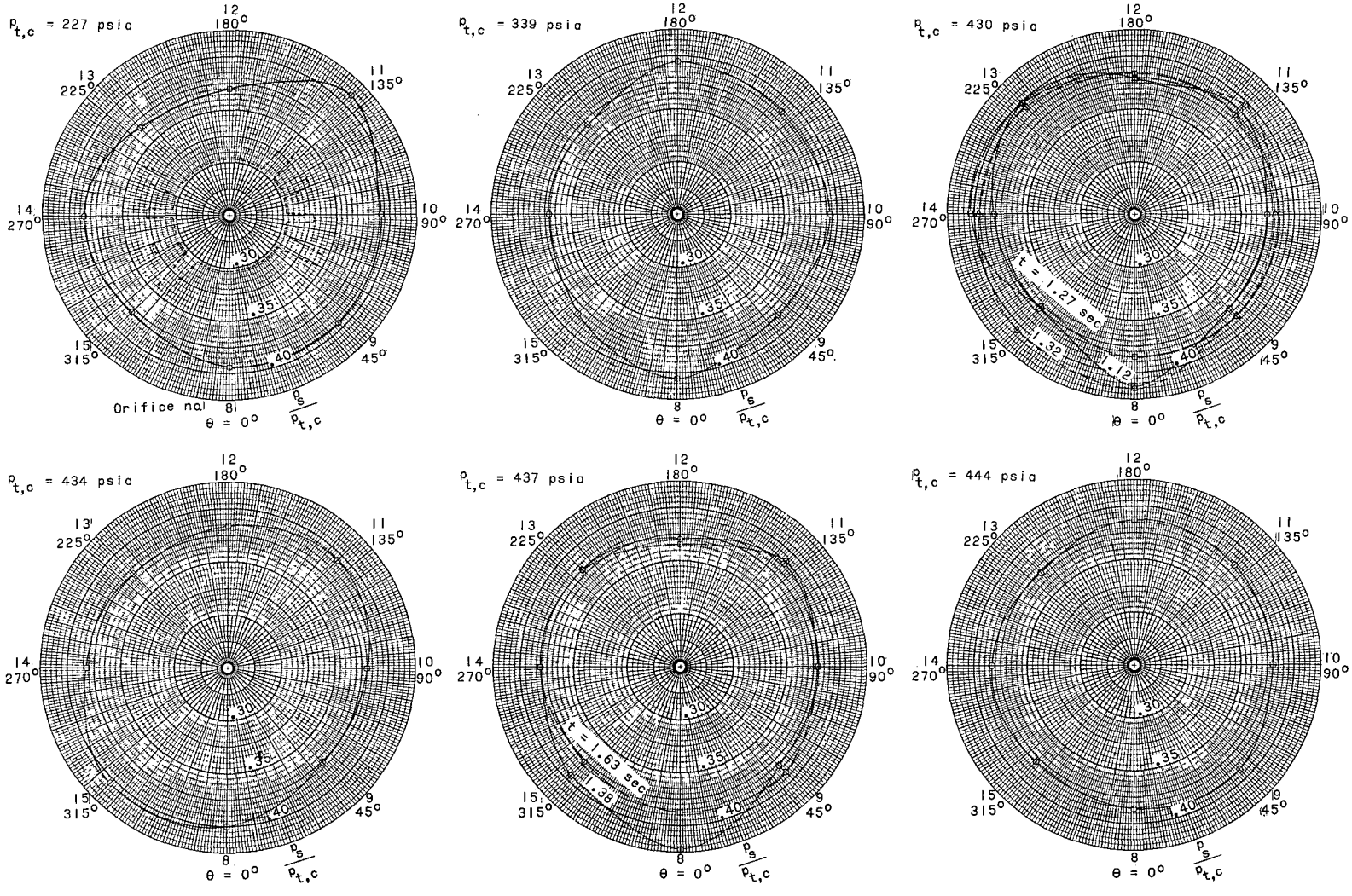

(a) Grain slots, clean nozzle.

Figure 7.- Static-pressure distributions about the periphery of the nozzle throat from airflow tests.

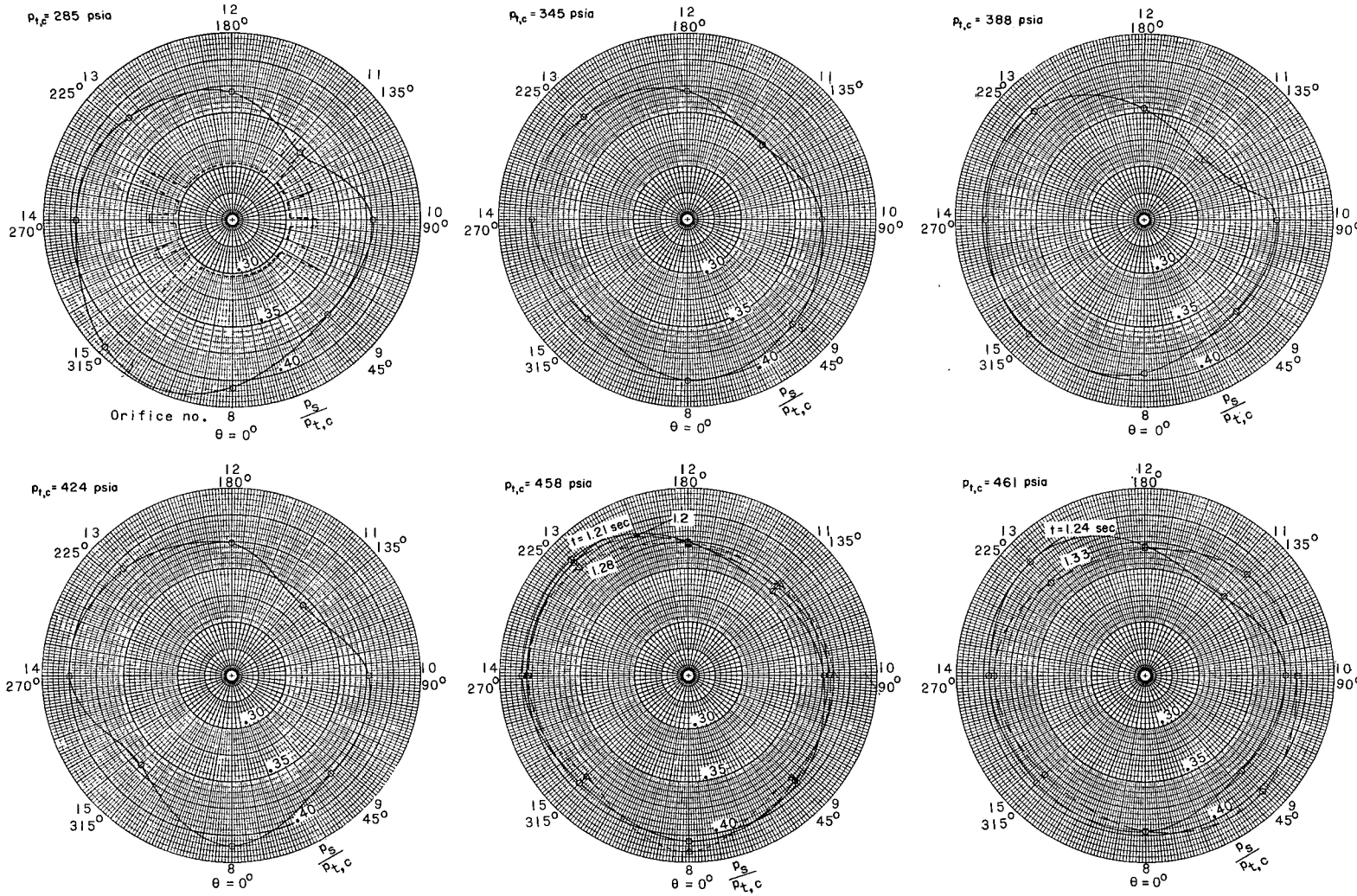

(b) Grain slots, residue on nozzle.

Figure 7.- Continued.

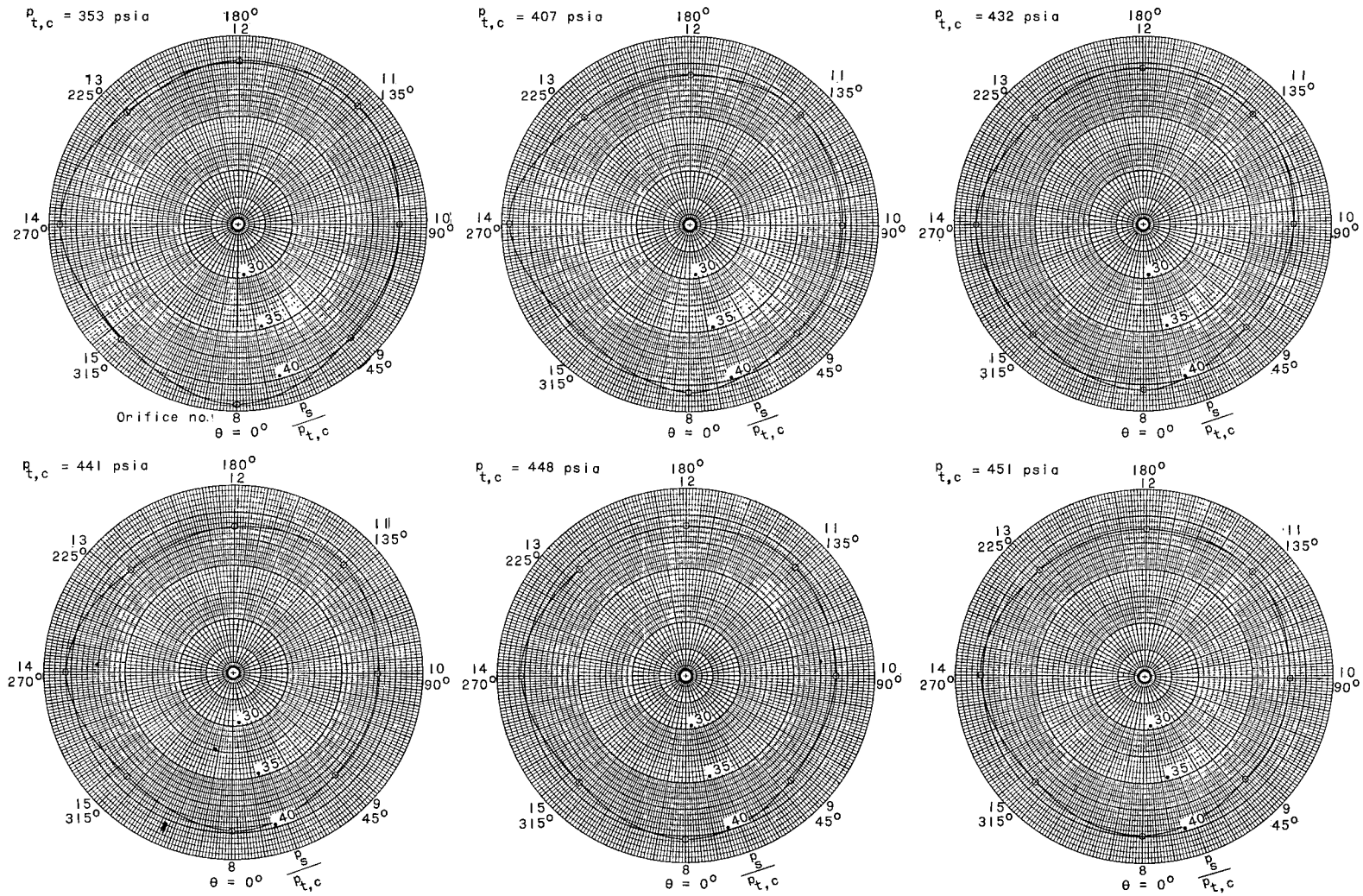

(c) No grain slots, clean nozzle.

Figure 7.- Concluded.

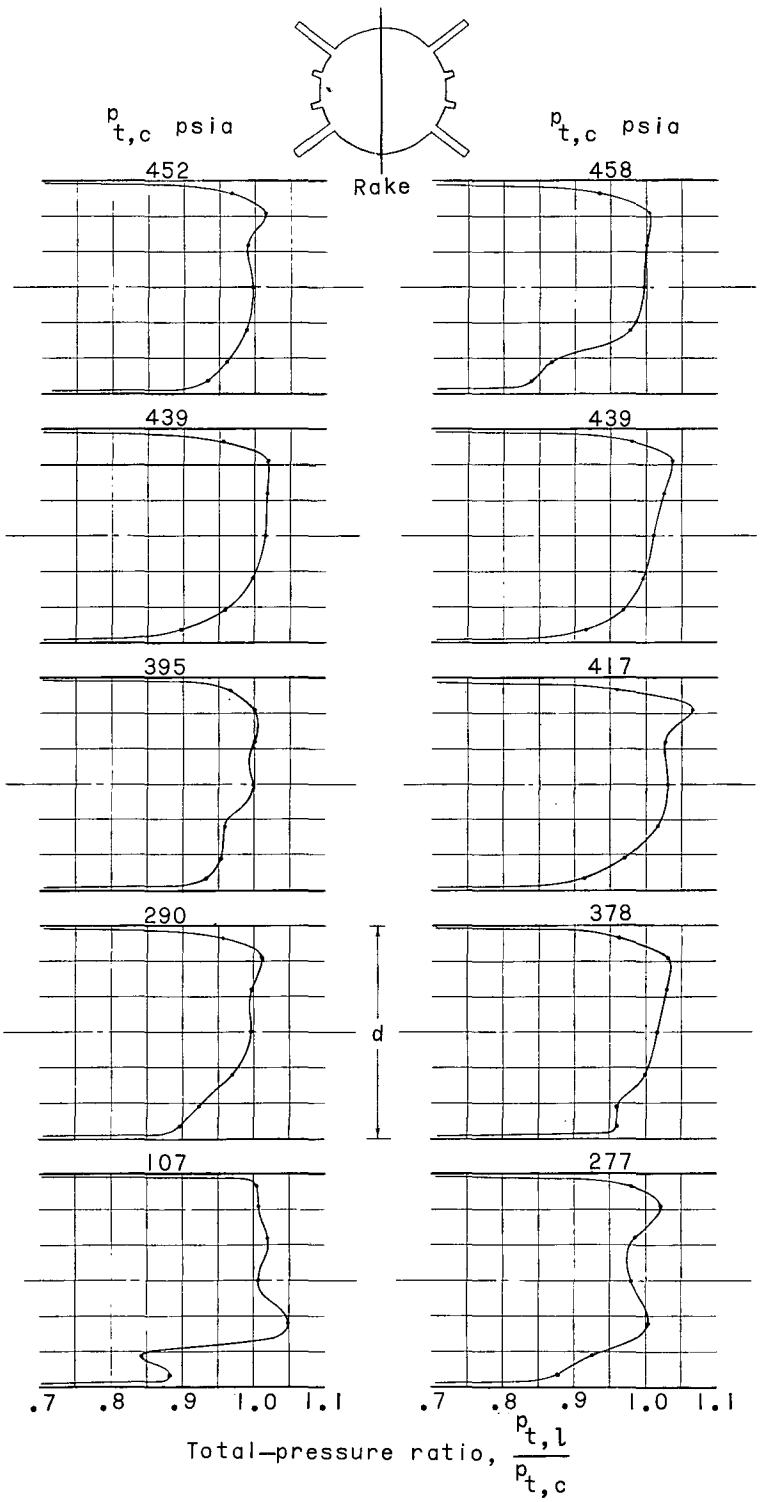

(a) Rake alined with center of grain unslotted region.

Figure 8.- Total-pressure distribution immediately downstream of the nozzle throat.

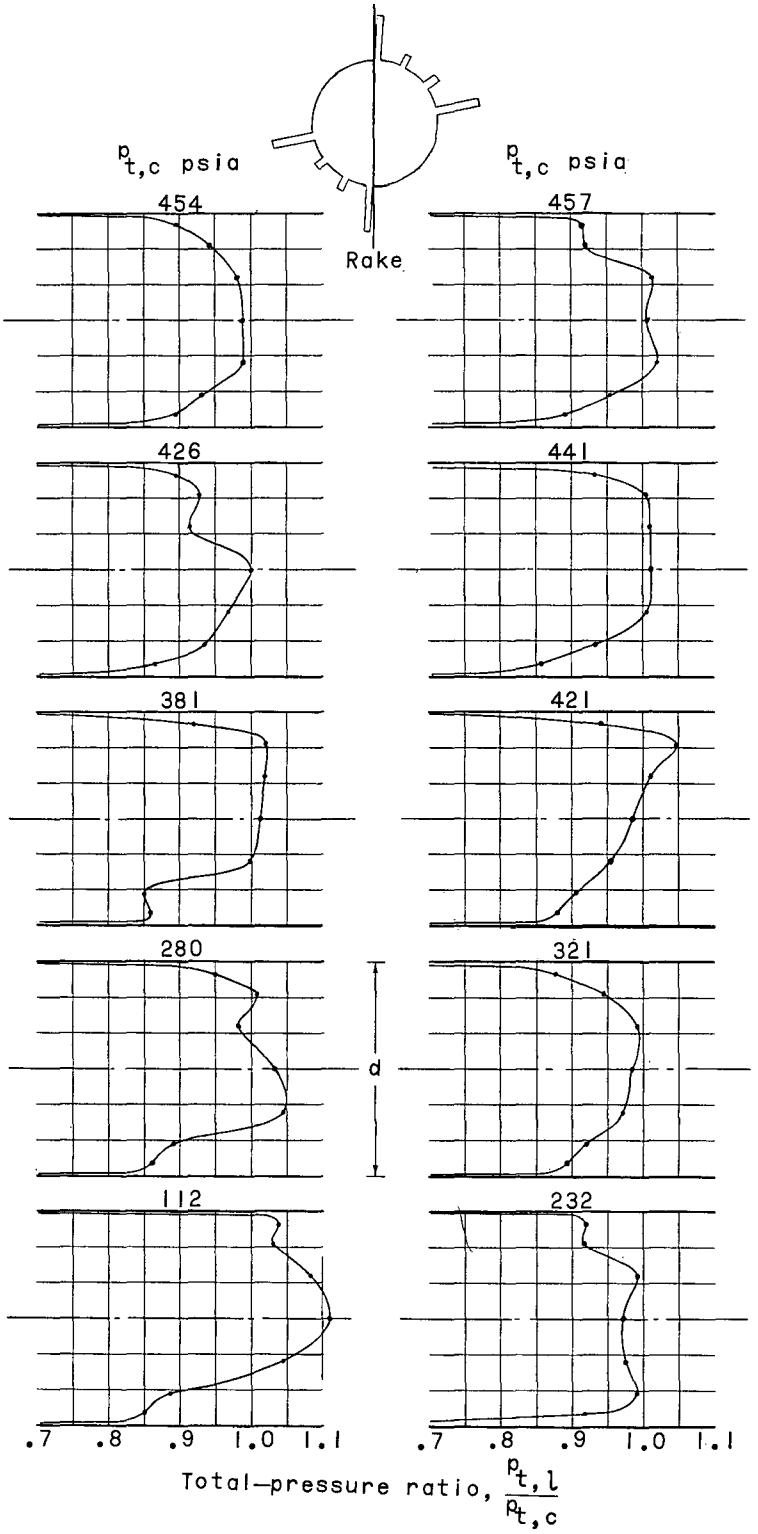

(b) Rake alined with deep slots of grain.

Figure 8.- Continued.

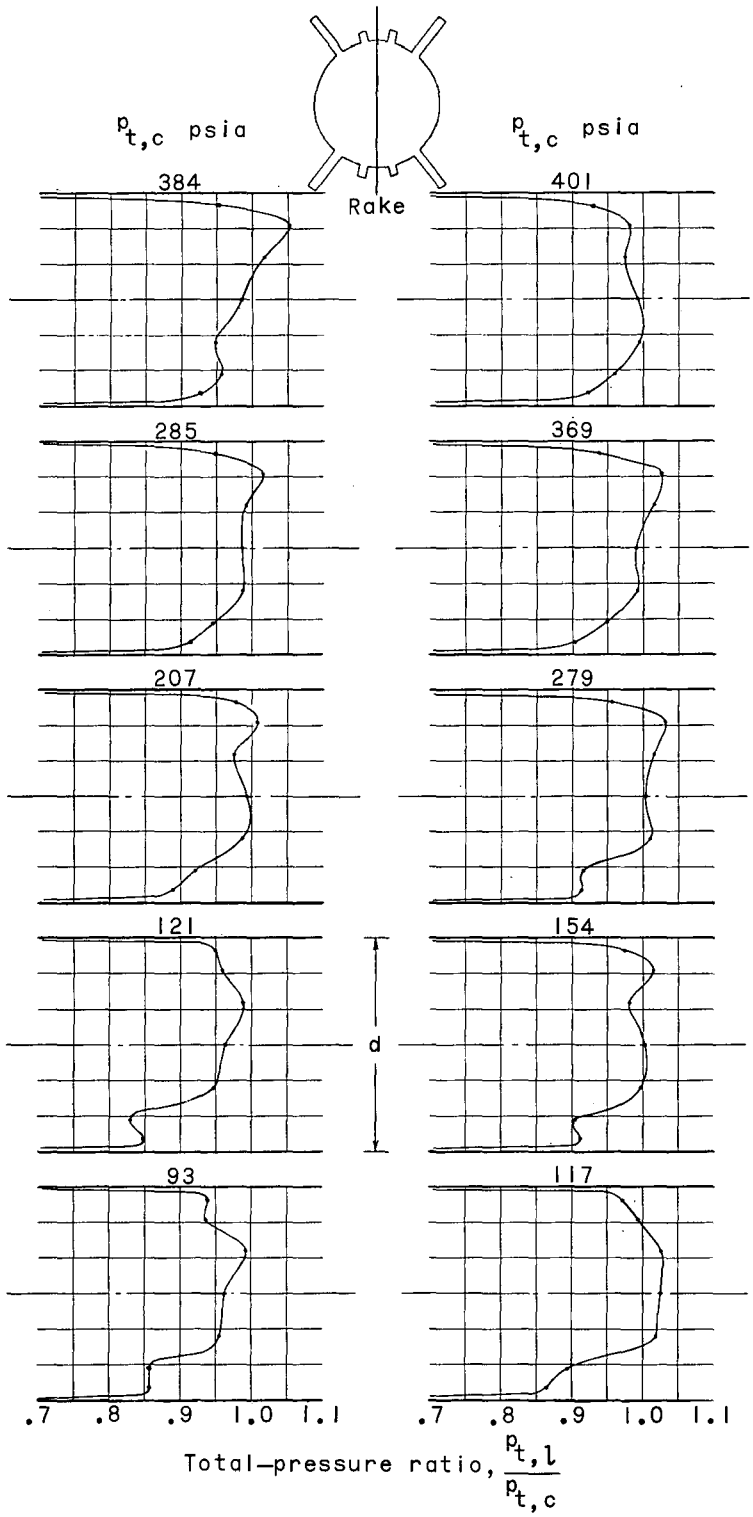

(c) Rake alined with center of grain slotted region.

Figure 8.- Concluded.

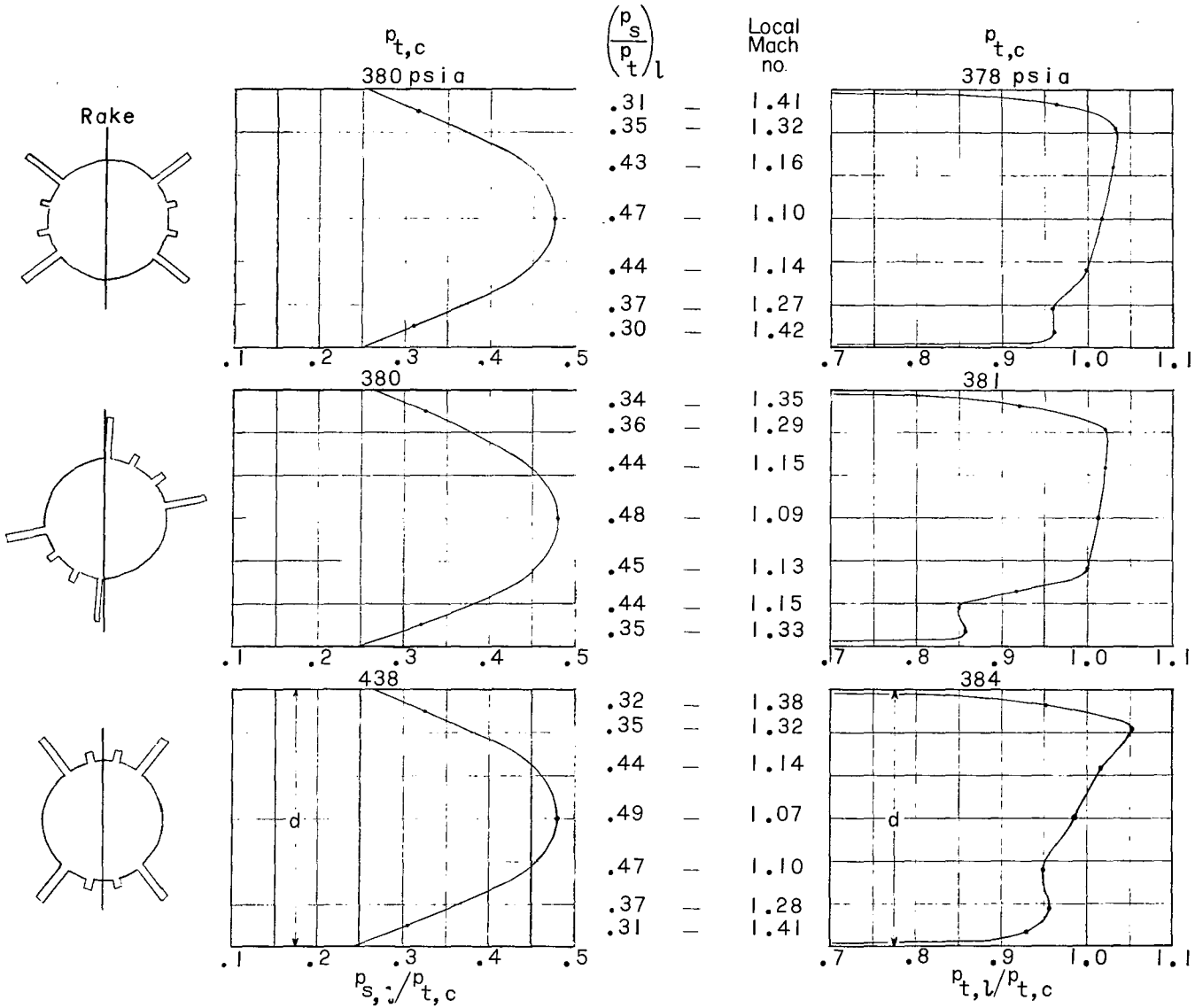

(a) Distributions of static- and total-pressure ratios.

Figure 9.- Static- and total-pressure distributions just downstream of the nozzle throat.

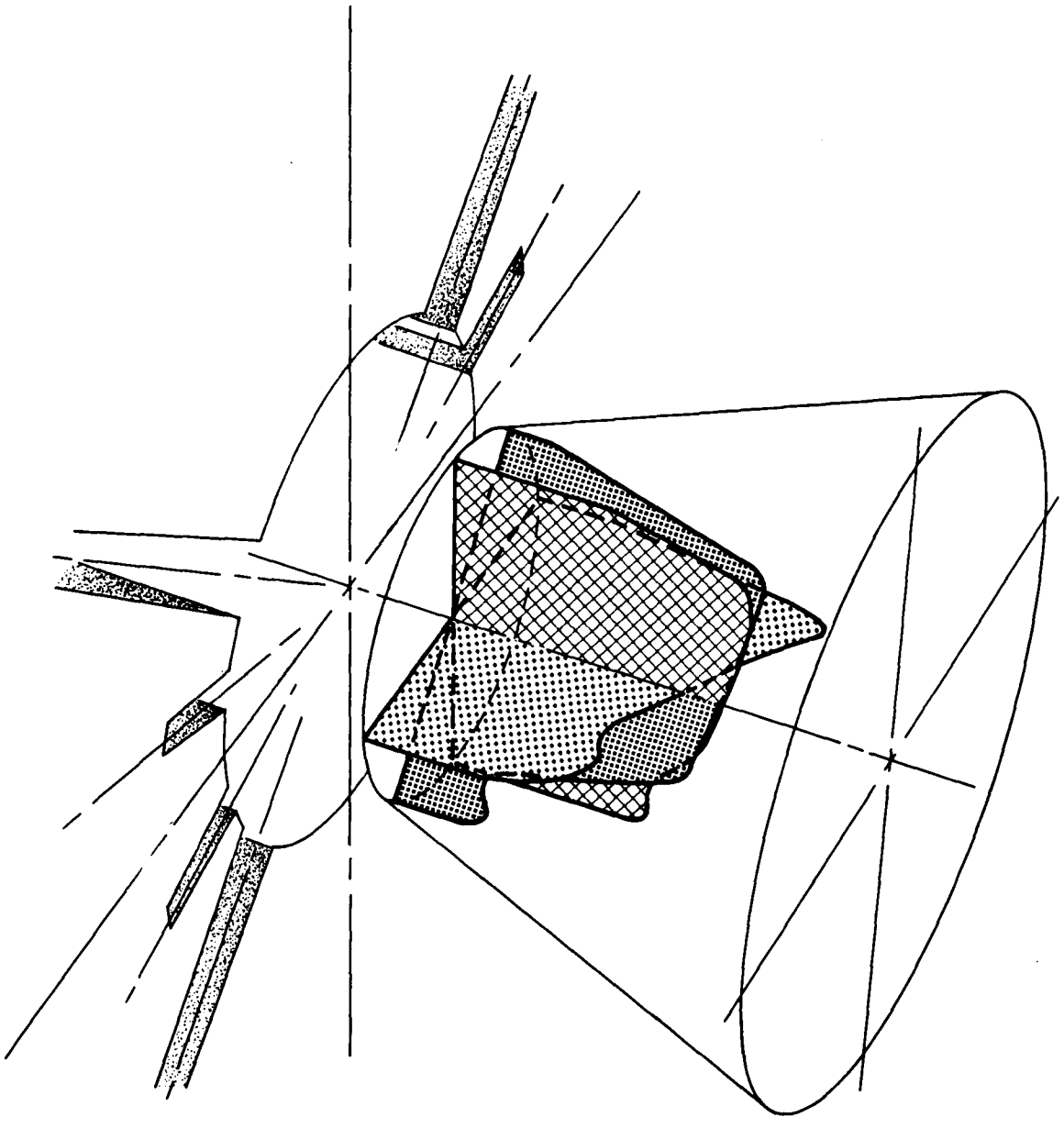

(b) Contour sketch of local-to-chamber total-pressure ratios. $\overline{p_{t,c}}$ = 381 psia.

Figure 9.- Concluded.

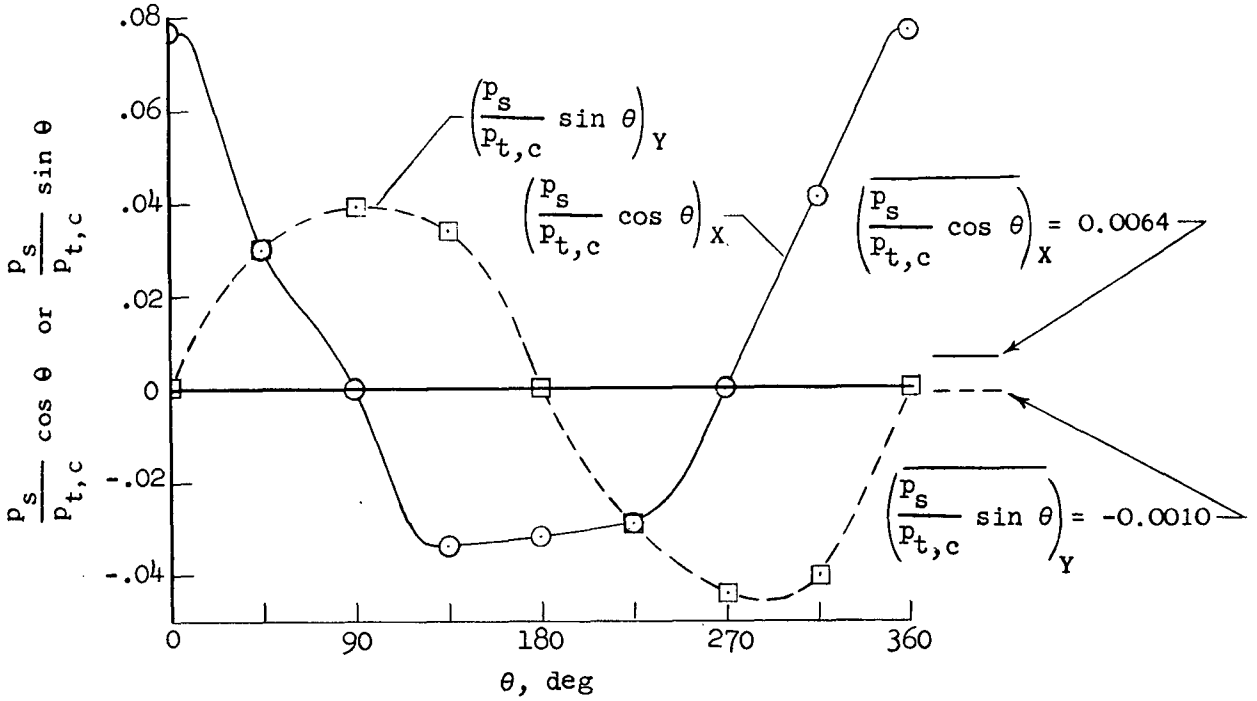

Figure 10.- Typical components of nozzle wall pressures along X- and Y-axes; throat station, t = 1.37 sec.

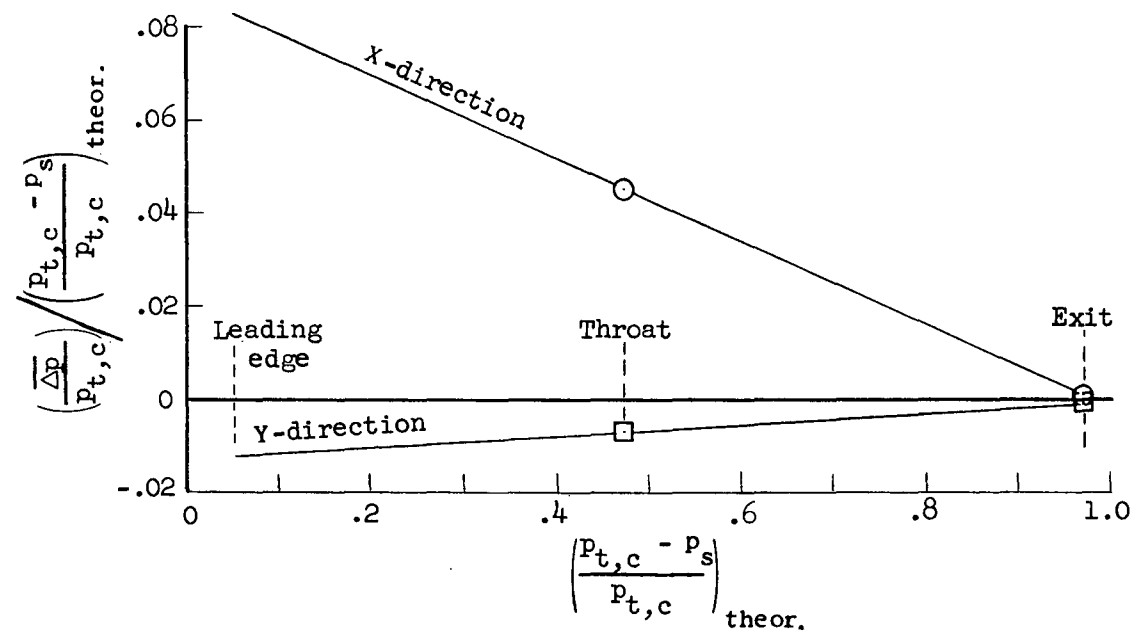

Figure 11.- Typical linear extrapolation along length of nozzle; t = 1.37 sec.

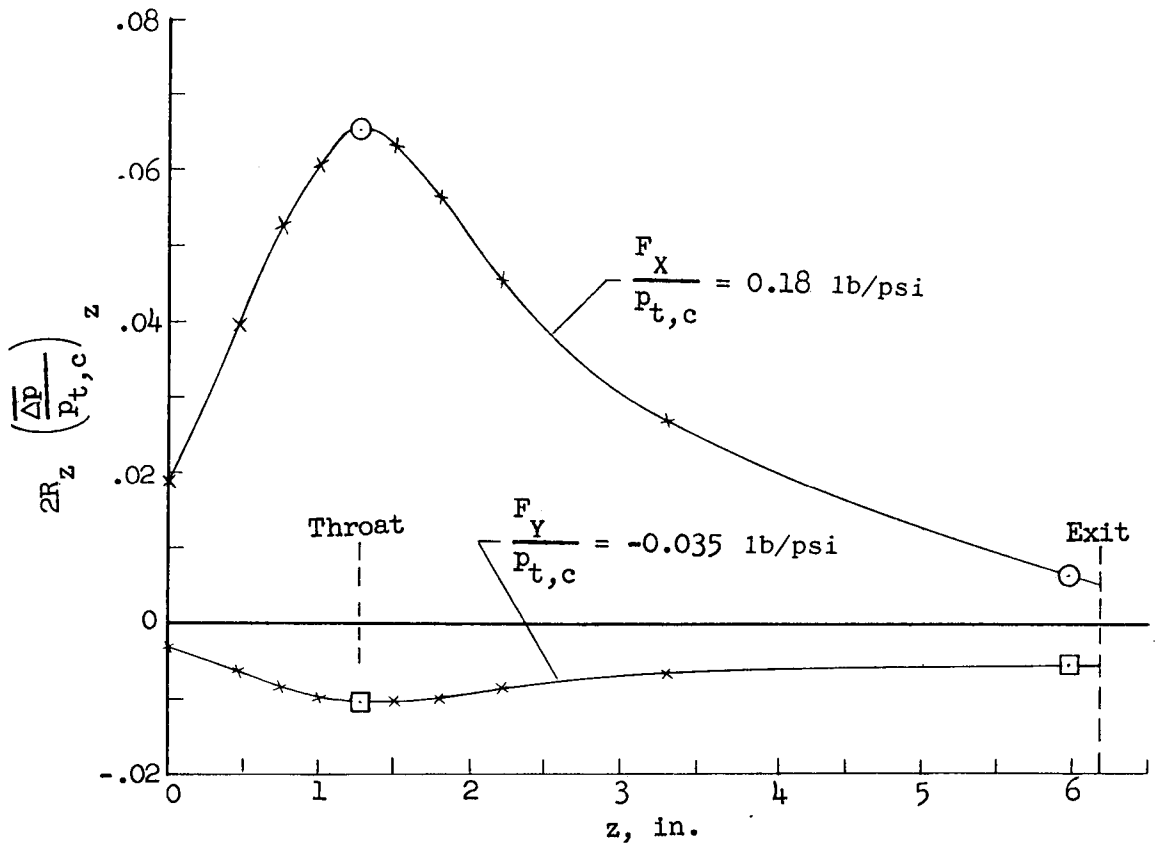

Figure 12.- Typical X- and Y-components of radial forces; t = 1.37 sec.

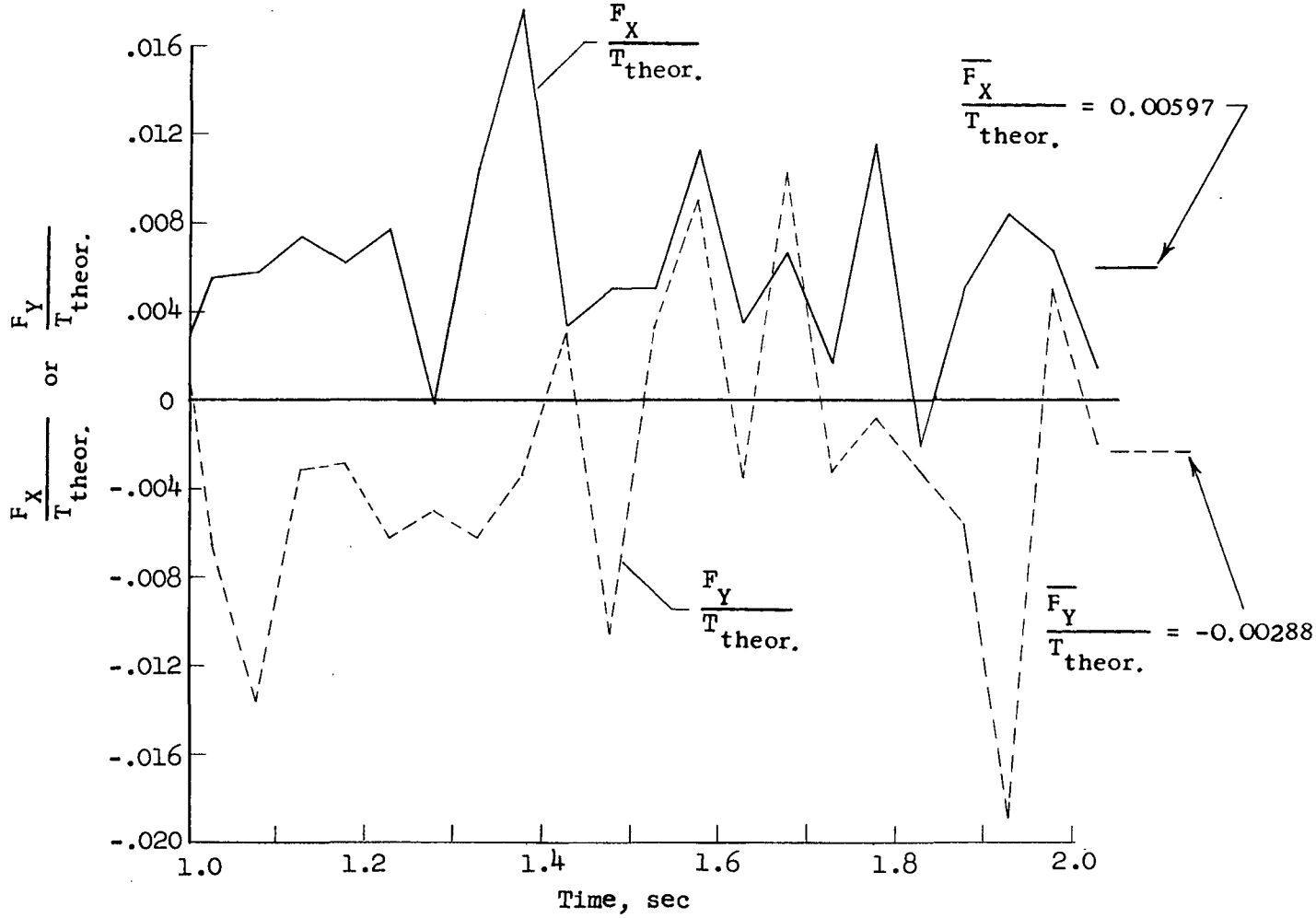

Figure 13.- Variation of radial-force components with respect to time.

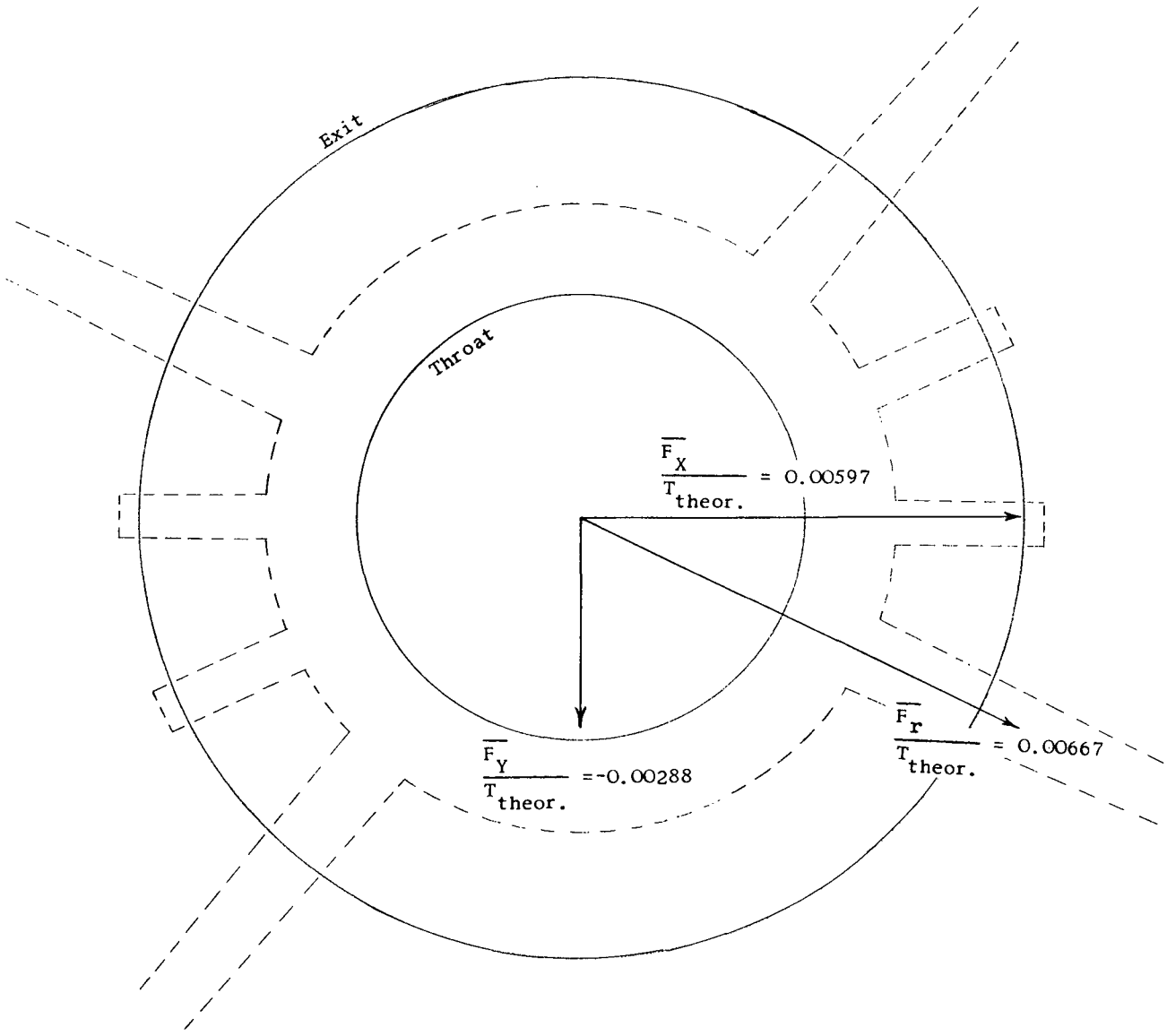

Figure 14.- Resultant side forces; grain-slot arrangement superimposed.

$\overline{p_{t,c}}$ = 425.49 psia and $\frac{\overline{T_{theor.}}}{p_{t,c}}$ = 10.35 lb/psi.

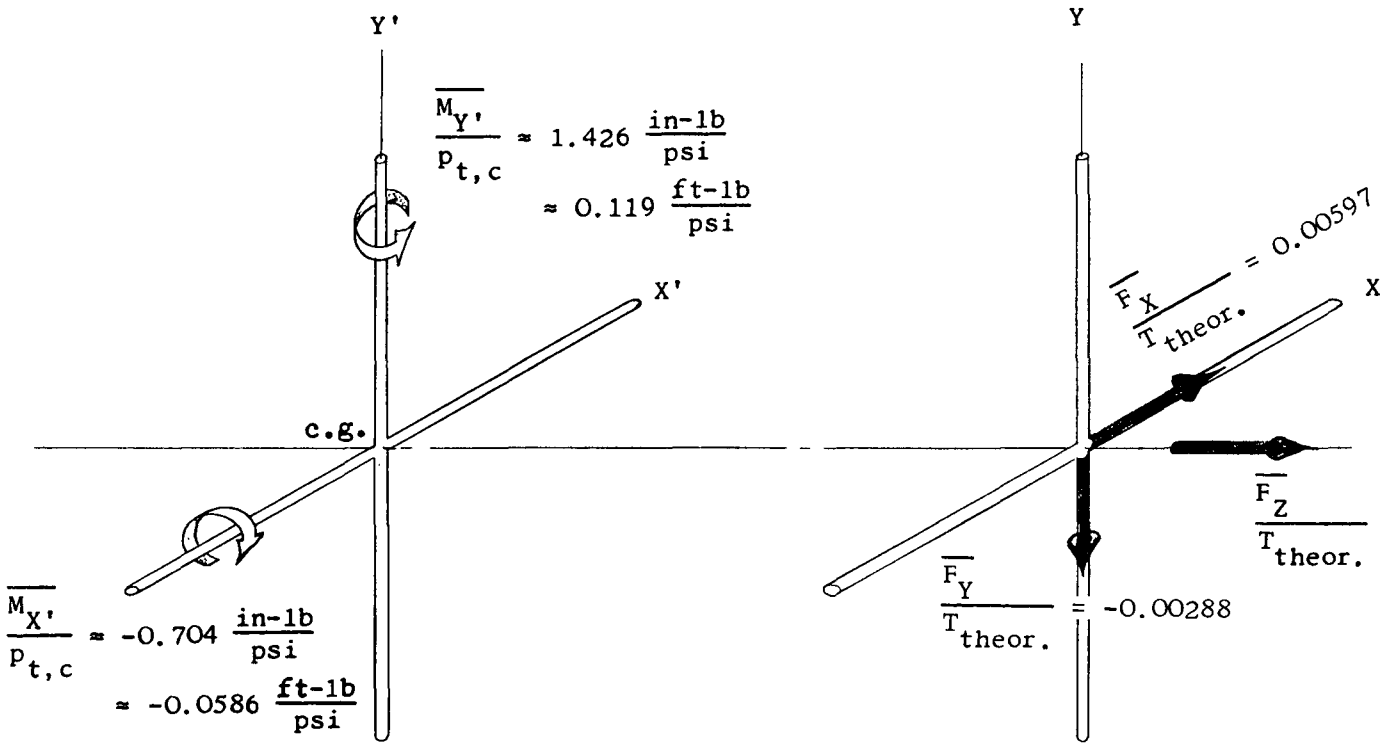

Figure 15.- Summary of the forces and moments contributing to tipoff.

$\frac{\overline{M_r}}{p_{t,c}} \approx 0.1325$ ft-lb/psi and $\frac{\overline{T_{theor.}}}{p_{t,c}} = 10.35$ lb/psi.

"The aeronautical and space activities of the United States shall be conducted so as to contribute . . . to the expansion of human knowledge of phenomena in the atmosphere and space. The Administration shall provide for the widest practicable and appropriate dissemination of information concerning its activities and the results thereof."

—NATIONAL AERONAUTICS AND SPACE ACT OF 1958

NASA SCIENTIFIC AND TECHNICAL PUBLICATIONS

TECHNICAL REPORTS: Scientific and technical information considered important, complete, and a lasting contribution to existing knowledge.

TECHNICAL NOTES: Information less broad in scope but nevertheless of importance as a contribution to existing knowledge.

TECHNICAL MEMORANDUMS: Information receiving limited distribution because of preliminary data, security classification, or other reasons.

CONTRACTOR REPORTS: Technical information generated in connection with a NASA contract or grant and released under NASA auspices.

TECHNICAL TRANSLATIONS: Information published in a foreign language considered to merit NASA distribution in English.

TECHNICAL REPRINTS: Information derived from NASA activities and initially published in the form of journal articles.

SPECIAL PUBLICATIONS: Information derived from or of value to NASA activities but not necessarily reporting the results of individual NASA-programmed scientific efforts. Publications include conference proceedings, monographs, data compilations, handbooks, sourcebooks, and special bibliographies.

Details on the availability of these publications may be obtained from:

SCIENTIFIC AND TECHNICAL INFORMATION DIVISION

NATIONAL AERONAUTICS AND SPACE ADMINISTRATION

Washington, D.C. 20546